CATALYTIC MECHANISM AND REDOX PROPERTIES OF HUMAN MANGANESE SUPEROXIDE DISMUTASE

By

VINCENT J.-P. LÉVÊQUE

A DISSERTATION PRESENTED TO THE GRADUATE SCHOOL
OF THE UNIVERSITY OF FLORIDA IN PARTIAL FULFILLMENT
OF THE REQUIREMENTS FOR THE DEGREE OF
DOCTOR OF PHILOSOPHY

UNIVERSITY OF FLORIDA

2000

To my parents, Jean-Yves and Christiane, whose love and guidance has always fueled my ambition and helped me overcome difficulties in life.
To my sister, Valerie, for all her support and confidence in both the worst and best times of my life.

ACKNOWLEDGMENTS

I would like to thank my mentors, Dr. David N. Silverman and Dr. Harry S. Nick, for their continuous support throughout my career in graduate school. They have provided me with excellent mentorship, continuous financial and personal support, and have taught me how to walk on my own in the scientific field. I also would like to acknowledge my committee members, Drs. Daniel L. Purich, Arthur S. Edison, and Benjamin A. Horenstein, for all their input and suggestions. I am also very grateful to my labmates for their time and helpful experience. I am especially thankful to Kristi Totten for her help and support well beyond her duties, and to Chris Davis for his countless advice, patience when answering multiple questions, and for his cheerfulness and good laughs especially during the worst times. I would also like to acknowledge Dr. Cua (Euro-American-Institute, Sophia-Antipolis, France) and Dr. Wells (Florida Institute of Technology, Melbourne, FL) for believing in me, motivating me, and opening my eyes to the world of science. Last, but not least, I would like to thank my family to which this dissertation is dedicated. Despite the distance that has separated us during my education in the United States, their continuous and truthful interest in my success has given me the strength to always push my goals a little further and to reach well beyond what I expected.

TABLE OF CONTENTS

page

ACKNOWLEDGMENTS iii

LIST OF TABLES vi

LIST OF FIGURES vii

ABSTRACT ix

CHAPTERS

1. INTRODUCTION 1

Oxygen Toxicity and Free Radicals 1
The Cellular Defense Against Free Radicals 2
Role of Mn-SOD 4
Structure of Mn-SOD 6
Catalytic Activity of Human Mn-SOD 8

2. THE ROLE OF GLUTAMINE 143 12

Introduction 12
Materials and Methods 14
Mutagenesis and Cloning 14
Transfer of the hMn-SOD cDNA from the phMnSOD4 clone to the pTrc 99A vector 14
Generation of human Mn-SOD site-directed mutants 15
Bacterial Growth and Protein Expression 17
Crystallography of Q143A Mn-SOD 18
Differential Scanning Calorimetry 19
Stopped-Flow Spectrophotometry 19
Single wavelength apparatus 19
Diode array spectrophotometer 21
Pulse Radiolysis 22
Results 22
Structure and Spectroscopy. 22
Catalysis 26
Differential Scanning Calorimetry. 29
Discussion 33

3. THE ROLE OF HISTIDINE 30 39

Introduction 39
Materials and Methods 40
Mutagenesis and Cloning 40
Bacterial Growth and Protein Expression 41
Crystallography of H30N Mn-SOD 41
Differential Scanning Calorimetry 42
Stopped-flow Spectrophotometry 42
Results 43
Structure of H30N Mn-SOD 43
Catalytic Properties of His 30 Mutant Enzymes 45
Thermal Stability 49
Discussion 51

4. REDOX PROPERTIES OF HUMAN MANGANESE SUPEROXIDE DISMUTASE 54

Introduction 54
The Need for Mediators 55
Determining the Extinction Coefficient of Human Mn-SOD 56
Measuring the Redox Potential of Human Mn-SOD 58
Materials and Methods 59
Gene Cloning and Protein Expression 59
Metal Analysis 60
Potentiometric Measurements of Human Mn-SOD 60
Instrumentation 60
Mediators 61
Single point experiments 63
Redox titration 64
Results 65
Extinction Coefficient of Human Mn-SOD and Mediators 65
Self mediation of human Mn-SOD 65
Mediators 66
Single point experiments 69
Redox titration 74
Discussion 78

5. CONCLUDING REMARKS AND FUTURE DIRECTIONS 85

REFERENCES 93

BIOGRAPHICAL SKETCH 100

LIST OF TABLES

Table — Page

Table 2-1: Values of the pH-independent steady-state kinetic constants for the dismutation of superoxide catalyzed by wild-type human Mn-SOD and mutants at position 143.[a] 28

Table 2-2: Transition temperatures for the unfolding of wild type human Mn-SOD and mutants at position 143. 32

Table 2-3: Values of the zero-order rate constant $k_0/[E_o]$ describing the product-inhibited phase, and rate constants k_5 and k_{-5} (of eq. 4) for the formation and dissociation of the product-inhibited complex, during the decay of superoxide catalyzed by human wild-type and Q143A Mn-SOD..... 36

Table 3-1: Steady-state kinetic constants for the decay of superoxide catalyzed by human Mn-SOD and mutants at pH 9.4 or 9.6 and 20 °C [a] 48

Table 3-2: Main unfolding transitions (Tm) for the reversible unfolding of native human Mn-SOD and mutants at position 30..... 50

Table 4-1: Potential mediators tested for the electrochemical titration of human Mn-SOD. Only $Fe(CN)_6$ and $Fe(CN)_5NH_3$ were appropriate mediators for human Mn-SOD. 70

Table 4-2: Midpoint redox potentials (E_m) and extinction coefficients (ε, oxidized form) of mediators used in this study to measure the midpoint potential of human Mn-SOD. Each wavelength ("signature peak") represents a peak of absorbance characteristic of the mediator. 71

Table 4-3: Intrinsic redox potentials obtained in this study through single point (S.P.) and reductive titrations..... 84

LIST OF FIGURES

Figure Page

Figure 1-1: The active site of human Mn-SOD from the data of Borgstahl et al. (1992). .. 7

Figure 1-2: Superoxide decay catalyzed by human Mn-SOD as determined by pulse radiolysis. 11

Figure 2-1: Scheme of the PCR reactions performed to generate point mutations in the Mn-SOD gene. 16

Figure 2-2: Schematic of the single wavelength stopped-flow apparatus..... 20

Figure 2-3: (a) The crystal structure of tetrameric human wild type Mn-SOD with subunits shown in different colors (Borgstahl et al., 1992). (b) The active site region from the crystal structure of the Q143A mutant. (c) Superposition of the active-site regions from the crystal structures of the wild-type human Mn-SOD and the Q143A mutant. 23

Figure 2-4: The visible absorbance spectra of wild-type human Mn-SOD and site-specific mutants Q143A, Q143H, and Q143N measured at pH 7.8 and 20 °C... 25

Figure 2-5: Superoxide decay catalyzed by Q143A Mn-SOD following introduction of superoxide by pulse radiolysis at 25 °C..... 27

Figure 2-6: The emergence and decay of the absorbance at 420 nm (pathlength 2.0 cm) of Q143A Mn-SOD following the introduction of 13 μM superoxide by pulse radiolysis. 30

Figure 2-7: Change in extinction coefficient ε ($M^{-1}cm^{-1}$) as a function of wavelength obtained by extrapolation of the decreasing phase of absorbance to the initial time of mixing of superoxide and Q143A Mn-SOD..... 31

Figure 3-1: The least-squares superposition of the crystal structures of wild-type human Mn-SOD and H30N Mn-SOD showing residues in the active-site..... 44

Figure 3-2: The initial velocities (μMs^{-1}) of the catalyzed decay of superoxide at 20 °C... 46

Figure 3-3: The logarithm of k_{cat}/K_m ($M^{-1}s^{-1}$) for the decay of superoxide catalyzed by wild-type human Mn-SOD and H30N Mn-SOD measured by stopped-flow at 20 °C. 47

Figure 4-1: Anaerobic cell engineered in our laboratory for all potentiometric measurements. 62

Figure 4-2: Reductive titration of human Mn-SOD by dithionite without a mediator. 67

Figure 4-3: Oxidation of Mn-SOD with permanganate. 68

Figure 4-4a: Single point titration of human Mn-SOD with $Fe(CN)_6$. 72

Figure 4-4b: Single-point titration of human Mn-SOD with $Fe(CN)_6$. 73

Figure 4-5: Single point titration of human Mn-SOD with $Fe(CN)_5NH_3$. 75

Figure 4-6a: Reductive titration of human Mn-SOD with dithionite using $Fe(CN)_6$ as a mediator. 76

Figure 4-6b: Absorbance of human Mn-SOD at 485 nm versus potential. 77

Figure 4-7a: Oxidative titration of human Mn-SOD with permanganate using $Fe(CN)_6$ as a mediator. 79

Figure 4-7b: Absorbance at 485 nm of human Mn-SOD versus ambient potential. 80

Figure 5-1: Overlay spectra of pulse radiolysis traces of wild type (WT), Gln143Ala (Q143A), and His30Asn (H30N) human Mn-SOD. 87

Abstract of Dissertation Presented to the Graduate School
of the University of Florida in Partial Fulfillment of the
Requirements for the Degree of Doctor of Philosophy

CATALYTIC MECHANISM AND REDOX PROPERTIES OF HUMAN MANGANESE SUPEROXIDE DISMUTASE

By

Vincent J.-P. Lévêque

August 2000

Chairman: Dr. David N. Silverman
Major Department: Biochemistry and Molecular Biology

Human manganese superoxide dismutase (Mn-SOD) is a detoxifying enzyme in mitochondria that converts superoxide ($O_2^{\cdot-}$) into oxygen (O_2) and hydrogen peroxide (H_2O_2). This reaction requires proton and electron transfer between the active site metal, and superoxide. Although it is catalytically very active, human Mn-SOD quickly becomes product-inhibited by peroxide. The goal of this work is to use site-specific mutagenesis and characterization of the resulting mutants to understand the role in catalysis and inhibition of two prominent active-site residues, Histidine 30 (His30) and Glutamine 143 (Gln143). To do so, I used a variety of techniques including X-ray crystallography, scanning calorimetry, pulse radiolysis, and stopped-flow spectrophotometry, performed in our laboratory and through collaborations. In addition, I

designed, ordered, and installed the appropriate equipment to measure the redox potential of human Mn-SOD in our laboratory.

Crystallography showed that mutations at both sites 30 and 143 interrupted the hydrogen-bonded network around the metal which possibly affected proton transfer during catalysis. The mutant His30Asn remained uninhibited during catalysis and could eliminate superoxide more efficiently than the wild type enzyme. Mutations at position 143 had a profound effect on both the kinetics of the enzyme and the redox state of the active site metal. Gln143 mutants were not product inhibited but were slower than wild type by two to three orders of magnitude, and mutations at this site altered the redox state of the enzyme.

The midpoint potential of human Mn-SOD was measured both through single point equilibrium and redox titration. The two methods yielded agreeable values with E_m = 393 ± 35 mV. This value lies at mid distance between the reduction and oxidation midpoint potentials of superoxide, which facilitates both reactions.

Therefore, Gln143 and His30 are required for rapid catalysis but are not essential for activity. Gln143 stabilizes manganese in the oxidized state and contributes to the fine-tuning of the redox potential which is required for efficient catalysis. His30 is involved in the formation of the product-inhibited complex in wild type human MnSOD; this inhibition is abolished in the mutant His30Asn. Therefore, this mutant is a good candidate for gene therapy research to provide better cytoprotection under states of oxidative stress.

CHAPTER 1
INTRODUCTION

Oxygen Toxicity and Free Radicals

Superoxide ($O_2^{\cdot -}$) is produced in all aerobic organisms during normal enzymatic activity and spontaneous oxidation (DiGuiseppi and Fridovich, 1984; Fridovich, 1985). Hyperoxia, activation of granulocytes and macrophages, conversion of hypoxanthine to xanthine during purine catabolism, and exposure to ionizing radiation are a few examples of superoxide related pathology (Bannister et al., 1987). The superoxide radical is unstable in an aqueous environment and spontaneously dismutes to O_2 and H_2O_2 in a pH dependent manner. The rate of spontaneous dismutation of $O_2^{\cdot -}$ is maximum at pH 4.8, the pKa of the conjugate acid $HO_2^{\cdot}$, and is accurately described by the rate law for spontaneous dismutation (Bull and Fee, 1985):

$$\frac{d[O_2^{\cdot -}]}{dt} = k_1[O_2^{\cdot -}] + 2k_2[O_2^{\cdot -}]^2 \qquad (1\text{-}1)$$

where k_1 corresponds to the superoxide dismutation due to free ions in solution, and k_2 corresponds to the autodismutation of superoxide. At pH 7.4, the second order rate constant of spontaneous dismutation is about $2 \times 10^5\ M^{-1}s^{-1}$. H_2O_2 is therefore present whenever $O_2^{\cdot -}$ is being produced in cells. Superoxide can also reduce transition metals such as Fe^{3+} or Cu^{2+}, the reduced forms of which can, in turn, reduce H_2O_2 to generate the devastatingly powerful oxidant $HO^{\cdot}$. This process is called the metal-catalyzed Haber-Weiss reaction (Beyer et al., 1991):

$$Fe^{3+} + O_2^{\cdot -} \leftrightarrows Fe^{2+} + O_2 \quad (1\text{-}2a)$$

$$Fe^{2+} + HOOH \leftrightarrows Fe^{1+}\text{–}OOH + H^+ \quad (1\text{-}2b)$$

$$Fe^{1+}\text{–}OOH \leftrightarrows Fe^{2+}\text{=}O + OH^- \quad (1\text{-}2c)$$

$$Fe^{2+}\text{=}O + H^+ \leftrightarrows Fe^{3+}\text{–}OH \leftrightarrows Fe^{3+} + HO^{\cdot} \quad (1\text{-}2d)$$

The hydroxyl radical and other highly reactive oxygen species have been proven to damage macromolecules including DNA by inducing base modifications and strand breakages (Imlay and Fridovich, 1992), proteins by causing breaks in the peptide backbone (Stadtman, 1991), and lipids by initiating lipid peroxidation (Gutteridge and Halliwell, 1990a) leading to chain reactions propagated with further exposure to O_2. In that last case, membrane integrity can be altered and may lead to deregulation of cellular processes and expulsion of cellular contents (including signaling molecules and free metal ions) resulting in a propagation of the damage through the whole tissue (Bruch and Thayer, 1983; Thompson and Hess, 1986). Free radicals have also been linked to reperfusion injury (Gutteridge and Halliwell, 1990b), diabetes, ageing processes and degenerative diseases including arthritis, cancers and arteriosclerosis (Kaprzak, 1991; Halliwell and Gutteridge, 1990; Cerutti, 1985; Cerutti and Trump, 1991; Homma et al., 1994).

The Cellular Defense Against Free Radicals

In response to the damaging effects of oxygen free radicals, organisms have developed an endogenous protective defense system that includes small molecule antioxidants like β-carotene, vitamins E and C. However, the primary defense of cells against the cytotoxic effects of reactive oxygen is provided by the antioxidant enzymes superoxide dismutase (SOD), catalase, and glutathione peroxidase (Frank and Massaro,

1980; Fridovich, 1985). SOD converts superoxide radicals into hydrogen peroxide and oxygen (Fridovich, 1978):

$$2O_2^{\cdot -} + 2H^+ \leftrightarrows O_2 + H_2O_2 \qquad (1\text{-}3)$$

Superoxide dismutase is an ubiquitous metalloenzyme in oxygen-tolerant organisms and has been classified according to the metal contained in the active site. Prokaryotic cells and cells in eukaryotes dismutate superoxide using up to four types of SODs containing either iron (Fe-SOD), manganese (Mn-SOD), or copper (Cu,Zn-SOD) in the active site (Fridovich, 1981). Recently, a nickel containing SOD has been isolated from *Streptomyces coelicolor* (Kim et al., 1996). The distribution of the different types of superoxide dismutases has been considered to reflect the evolutionary stage of the organism (Asada et al., 1977). Fe-SOD is thought to be the most primitive form of SOD due to its presence in anaerobic bacteria and in prokaryotes. The Mn-SOD is present in prokaryotes and mitochondria, but not in chloroplasts as once thought (Palma et al., 1986). Cu,Zn-SOD is found almost exclusively in eukaryotes, both intracellularly (Cu,Zn-SOD) and extracellularly (EC-SOD). However, the distribution pattern of the three classes of SOD is not so clearly defined. Indeed, Mn-SOD has also been isolated from anaerobic bacteria (Meier et al., 1982; Gregory, 1985), and some bacterial species contain a prokaryotic form of Cu,Zn-SOD (Martin et al., 1986; Puget and Michelson, 1974; Steinman, 1982, 1985) that is structurally unrelated to the eukaryotic form. Also, a survey indicates that Fe-SOD has been isolated from four plant species (Bridges and Salin, 1981; Salin and Bridges, 1982; Kwiatowski et al., 1985; Duke and Salin, 1985).

In humans, the nuclear encoded mitochondrial Mn-SOD protein is a homotetramer composed of 22 KDa subunits (Borgstahl et al., 1992; Wagner et al.,

1993). The amino-acid sequence of the mitochondrial Mn-SOD is highly homologous to the bacterial Mn-SOD and Fe-SOD, but does not resemble the cytosolic Cu,Zn-SOD present in eukaryotes. This observation provides additional support for the proposal that mitochondria originated as aerobic prokaryotes that went through an endocellular symbiotic process with protoeukaryotes to give rise to eukaryotes (Schnepf and Brown, 1972).

Role of Mn-SOD

The mitochondrial electron transport system consumes over 90% of the cell's oxygen. This oxygen is normally reduced to water during cellular respiration. However, even under normoxic conditions, approximately 1 to 5% of this oxygen escapes the respiratory chain and leaks out in the form of oxygen radicals (Chance et al., 1979). Free radicals are also generated through numerous cellular enzymatic reactions (DiGuiseppi and Fridovich, 1984) and are needed for essential processes such as prostaglandin synthesis (Kalyanaraman et al., 1982). Fridovich and coworkers first demonstrated that Mn-SOD, by converting $O_2^{\cdot -}$ into O_2 and H_2O_2, is the principal source of oxygen free radical detoxification in mitochondria in both physiological and pathological conditions. The absence of SOD in anaerobic prokaryotes is lethal upon oxygen exposure (Fridovich, 1985) and the knockout of the *sodA* and *sodB* genes (coding respectively for Mn- and Fe-SOD) in E. coli, enhances the rate of oxygen-dependent mutagenesis (Farr et al., 1986), as well as the rate of an oxygen-dependent loss of viability at moderately elevated temperatures (Benov and Fridovich, 1995). Fridovich and coworkers demonstrated that hyperoxia induces SOD activity in bacteria and that microorganisms with elevated levels of SOD are resistant to a subsequent exposure of normally lethal levels of hyperbaric oxygen (Gregory and Fridovich, 1973).

Crapo and Tierney (1974) extended the involvement of SOD in developing hyperoxia tolerance to eukaryotes. They found that rats pre-exposed to an oxygen tension of 85% subsequently survive a normally lethal 100% oxygen environment at a higher rate. Other studies have shown that Mn-SOD expression (but not Cu,Zn-SOD) is induced by tumor necrosis factor (TNF) and interleukin-1 (IL-1) (Visner et al., 1992) and has protective effects on endothelial cells (Wong et al., 1991). SODs can therefore be used to ameliorate oxygen free radical-mediated lung toxicity (Padmanabhan et al., 1985).

Studies by Li et al. (1995) on homozygous mutant mice lacking both alleles of the Mn-SOD gene demonstrate the critical cellular importance of Mn-SOD in a variety of different tissues. These mutant mice die within 10 days of birth and exhibit severe dilated cardiomyopathy, accumulation of lipid in liver and skeletal muscle, metabolic acidosis, and decreased activities of aconitase, succinate dehydrogenase and cytochrome c oxidase. In humans, improper SOD function has been associated with amyotrophic lateral sclerosis (ALS) where a zinc misincorporation in Cu,Zn-SOD has been associated with motor neurone degradation by an oxidative mechanism involving $NO^{\cdot}$ (Rosen, 1995; Deng et al., 1995; Estévez et al., 1999). Improper SOD function has also been associated with Down syndrome where SOD expression level is high and out of balance with catalase (Summitt, 1981). Alteration in Mn-SOD levels have also been associated with a number of neurodegenerative diseases, including Parkinson's disease (Yoritaka et al., 1997; Bostantjopoulou et al., 1997), Duchenne muscular dystrophy (Mechler et al., 1984), Charcot-Marie-Tooth disease and Kennedy-Alter-Sung syndrome (Yahara et al., 1991). Therefore, Mn-SOD is extremely important as a main line of defense against oxidative damage.

Structure of Mn-SOD

A broad spectrum of techniques that includes X-ray crystallography has been used to study superoxide dismutase. The three-dimensional X-ray structures of Cu,Zn-SOD (Tainer et al., 1983), Fe-SOD (Stallings et al., 1983), and bacterial Mn-SOD (Stallings et al., 1985) have directly contributed to understanding the activity and biochemical properties of SODs. The crystal structure of human Mn-SOD has been determined at a 2.2 Å resolution (Borgstahl et al., 1992) and is a homotetramer, which contains a short α-helix per monomer (not present in dimeric SODs) to join the two dimers together and stabilize the tetramer. The crystal structure of tetrameric Mn-SOD from *Thermus thermophilus* has been determined at 2.4 Å (Stallings et al., 1985) and shows high levels of homology with the human enzyme. As its human homologue, *T. thermophilus* Mn-SOD also contains a short helix that is not found in dimeric Mn-SODs. The crystal structures of *E.coli* (Stalling et al., 1983) and *Pseudomonas ovalis* (Ringe et al., 1983) Fe-SODs, and yeast Mn-SOD (Beem et al., 1976) have similar structures to human Mn-SOD, which includes the same ligands and approximate geometry about the metal. There is no homology between the human Mn-SOD and Cu,Zn-SOD either in primary, secondary, or tertiary structures.

In human Mn-SOD, the geometry about the metal is trigonal bipyramidal with five ligands: three histidines (His 26, 74, 163), one aspartate (Asp 159) and a solvent molecule (water or hydroxide, see figure 1-1). There is an extensive hydrogen bonded network throughout the active site cavity involving first sphere (metal ligands) and part of which is shown in figure 1-1. This hydrogen-bonded network has been identified by

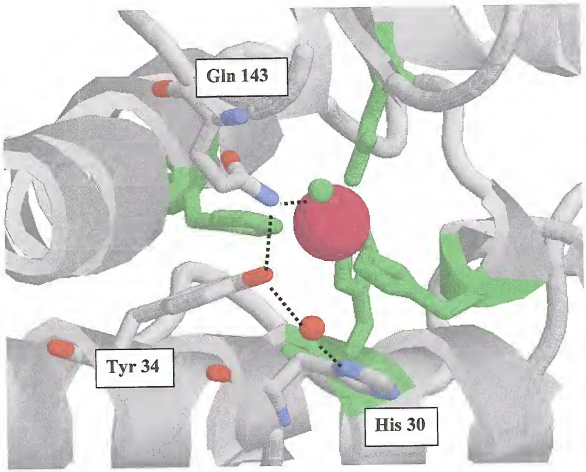


Figure 1-1: The active site of human Mn-SOD from the data of Borgstahl et al. (1992). Active site manganese is shown in spacefilling conformation (pink). Ligands to the manganese are His 26, 74, and 163, Asp 159, and a solvent molecule (green). Relevant second sphere residues are shown and include His 30, Tyr 34 and Glu 143 (CPK[1]). Backbone is shown in cartoon configuration (gray). Hydrogen bonds between second sphere residues are shown in doted lines. Image generated with Raswin 2.6 (Glaxo Wellcome Research and Development Stevenage, U.K.).

[1]The CPK color scheme is based upon the color of the model, which was developed by Corey, Pailing and Kultun. This color scheme attributes a specific color for each element (Carbon: light gray; Oxygen: red; Nitrogen: light blue).

crystallography (Guan et al., 1998; Borgstahl et al., 1992) and by proton NMR chemical shifts in *E. coli* Fe-SOD (Sorkin and Miller, 1997). In this network, the solvent ligand of manganese is hydrogen bonded to the side chain imidazole of His 30, which in turn forms two hydrogen bonds: one with the side-chain hydroxyl of Tyr 34 through a water molecule, and the other with the side chain hydroxyl of Tyr 166 from the adjacent subunit. A goal of this work is to determine if two of the residues involved in this hydrogen-bonded array, Glu 143 and His 30, are involved in proton transfer necessary for the formation of product hydrogen peroxide.

Catalytic Activity of Human Mn-SOD

The catalytic mechanism of Mn-SOD is not as well characterized as that of Cu,Zn-SOD. Pulse radiolysis studies on Cu,Zn-SOD (Fielden et al., 1974) reveal that catalysis is carried out through a relatively simple redox process in which the metal cycles between the oxidized and reduced state :

$$\text{Enz-Cu}^{2+} + O_2^{\cdot -} \leftrightarrows \text{Enz-Cu}^{1+} + O_2 \qquad (1\text{-}4)$$

$$\text{Enz-Cu}^{1+} + O_2^{\cdot -} + 2H^+ \leftrightarrows \text{Enz-Cu}^{2+} + H_2O_2 \qquad (1\text{-}5)$$

The catalytic rate of Cu,Zn-SOD is diffusion-controlled ($k_{cat}/K_m = 2 \times 10^9\ M^{-1}s^{-1}$), suggesting the evolution of an optimal active site for the recognition and chemical catalysis of $O_2^{\cdot -}$. The dismutation of superoxide catalyzed by Cu,Zn-SOD shows no evidence of saturation, so k_{cat} has not been determined. Conversely, Mn-SOD from *T. thermophilus* does show saturation kinetics, with $k_{cat} = 1.2 \times 10^4\ s^{-1}$ (Bull et al., 1991).

Details from kinetic studies on Mn-SOD from *Bacillus stearothermophilus* (McAdam et al., 1977a, 1977b) and *Thermus thermophilus* (Bull et al., 1991), which also involve alternate reduction and reoxidation of the active site metal, suggest a different and more complex catalytic mechanism from that involved in Cu,Zn-SOD. The

difference is primarily due to the rapid formation of an inactive form of the enzyme, designated as Enz-Mn^{3+}-X:

$$\text{Enz-Mn}^{3+} + O_2^{\cdot -} \underset{k_1}{\overset{k_{-1}}{\leftrightarrows}} [\text{ Enz-Mn}^{3+}\text{- } O_2^{\cdot -}] \xrightarrow{k_2} \text{Enz-Mn}^{2+} + O_2 \qquad (1\text{-}6)$$

$$\text{Enz-Mn}^{2+} + O_2^{\cdot -} + 2H^+ \underset{k_3}{\overset{k_{-3}}{\leftrightarrows}} [\text{ Enz-Mn}^{2+}\text{- } O_2^{\cdot -}] + 2H^+ \xrightarrow{k_4} \text{Enz-Mn}^{3+} + H_2O_2 \qquad (1\text{-}7)$$

$$k_5 \downarrow\uparrow k_{-5}$$

$$[\text{ Enz-Mn}^{3+}\text{-X }]$$

In this scheme, the *active* form of the enzyme follows the same mechanism as that of Cu,Zn-SOD presented earlier (1-4, 1-5). The enzyme, initially in the oxidized state, binds a superoxide molecule to form the complex Enz-Mn^{3+}- $O_2^{\cdot -}$ and is then reduced to release a dioxygen molecule. During the second half of the reaction, the enzyme binds a new superoxide molecule to form the complex Enz-Mn^{2+}- $O_2^{\cdot -}$. One peroxide molecule is then released and the enzyme reoxidized. Mn-SOD is unique in its ability to enter an inactive form through internal rearrangement of the Enz-Mn^{2+}- $O_2^{\cdot -}$ complex. This inactive form of the enzyme, resulting from the oxidative addition of $O_2^{\cdot -}$ to Mn^{2+}, is hypothesized to be a side-on peroxo complex, represented as Enz-Mn^{3+}-X in eq. 1-7 (Bull et al., 1991). This model is derived from inorganic systems in which peroxide is bound to Mn^{3+} in a side-on fashion (Lever and Gray, 1978):

$$Mn^{2+}(d^8) + O_2^{\cdot -} \longrightarrow Mn^{3+}(d^6) \begin{matrix} O \\ \diagup \\ \diagdown \\ O \end{matrix} \qquad (1\text{-}8)$$

For Mn-SOD, catalysis depends in part on the rate at which the inactive enzyme reverts to the active form (k_{-5}). The rate constant k_{-5} has a value around 70 s^{-1} in *B.*

stearothermophilus Mn-SOD (McAdam et al., 1977b) and 10 s^{-1} in *T. thermophilus* Mn-SOD (Bull et al., 1991).

Due to the rapid accumulation of the inactive form of the enzyme, the catalytic dismutation of superoxide by Mn-SOD takes place in two consecutive stages (Bull et al., 1991). The first stage (called the burst phase) is where the enzyme is most active, and catalysis by Mn-SOD follows simple Michaels-Menten kinetics. Within milliseconds under laboratory pulse radiolysis conditions, the enzyme is almost totally inactivated and the rate of superoxide disappearance becomes zero order.

Figure 1-2 shows the catalytic dismutation of $O_2^{\cdot -}$ radicals by human Mn-SOD and demonstrates the biphasic pattern including the initial activity (or burst phase) and subsequent zero-order decay of $O_2^{\cdot -}$. Hsu and coworkers also calculated the turnover number of human Mn-SOD with a simulated fit of the model of Bull et al. (1991) and found $k_{cat} = 4 \times 10^4\ s^{-1}$ and $k_{cat}/k_m = 8 \times 10^8\ M^{-1}s^{-1}$.

The purpose of this work is to elucidate the role of active site residues during catalysis of human Mn-SOD (chapters 2 and 3), and to measure the finely tuned redox potential of the active site metal (chapter 4). The unifying goal of this study is to understand how Mn-SOD achieves such a fast kinetic turnover, why it is so rapidly product inhibited, and how the enzyme adjusts the metal's redox potential to favor optimum catalysis. In the long term, by better understanding the connection between catalysis and product inhibition, this information could be utilized to develop therapeutic strategies for supplementing insufficient endogenous SOD levels with chimeric SODs with fast turnovers but freed from product inhibition.

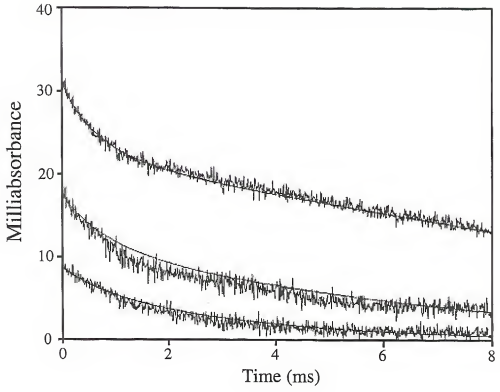


Figure 1-2: Superoxide decay catalyzed by human Mn-SOD as determined by pulse radiolysis. Data show the decrease in absorbance of superoxide at 250 nm (ε = 2000 $M^{-1}.cm^{-1}$) as a function of time. All solutions contained 0.5 mM Mn-SOD, 50 mM EDTA, 10 mM sodium formate, and 2.0 mM sodium pyrophosphate at pH 9.4 and 20 °C. Traces from the top of the figure down contain an initial concentration of superoxide of 11.6 μM, 6.5 μM and 3.4 μM respectively. The calculated lines shown in the figure are kinetics simulations (KINSIM) determined from the model of Bull et al. (1991).

CHAPTER 2
THE ROLE OF GLUTAMINE 143

Introduction

Site-directed mutagenesis has been used extensively to delineate catalytic mechanisms and pinpoint the role of active site residues in enzymes. In wild-type human Mn-SOD, five residues near the manganese (but not directly coordinated to the metal) have been found by site directed mutagenesis to influence the rate of catalysis; they are His 30 (Borders et al., 1998; Ramilo et al., 1999), Tyr 34 (Hunter et al., 1997; Sorkin and Miller, 1997; Whittaker and Whittaker, 1997; Guan et al., 1998); Gln 143 (Hsieh et al., 1998, Lévêque et al., 2000); Trp 161 (Cabelli et al., 1999), and Tyr 166 (Ramilo et al., 1999). Of these five sites, amino acid replacement at position 143 has the largest effect on catalytic activity. The amide of the side chain of Gln 143 forms a hydrogen bond with the manganese-bound solvent molecule and also with the hydroxyl side chain of Tyr 34. These residues form a hydrogen-bonded network that includes other solvent molecules and extends to other residues in the active-site cavity (Figure 2-3). Glutamine 143 is conserved in the majority of known eukaryotic Mn-SODs and in some bacterial forms of the enzyme (Smith and Doolittle, 1992). Replacing Gln 143 with Asn in human Mn-SOD caused a decrease of two to three orders of magnitude in catalytic activity compared with wild type (Hsieh et al., 1998). Also, unlike the wild type, which favors EPR silent Mn^{3+}-SOD in the resting state, Q143N favors Mn^{2+} in the resting state and has a complex EPR spectrum with many resonances in the region between 1200 and 2000 Gauss (Hsieh et al.,

1998). In addition, this mutant does not show a visible absorption spectrum typical of the wild-type Mn-SOD (Lévêque et al., 2000). These observations indicate a potential role of glutamine 143 in (1) maintaining maximum catalytic rate and (2) adjusting the redox potential of the manganese ion so that Mn^{3+} is stabilized in the resting state. Moreover, the mutant Q143N Mn-SOD was reported to have no significant product inhibition (Hsieh et al., 1998), and all mutant enzymes at this site follow Michaelis-Menten kinetics (Lévêque et al., 2000). However, the product-inhibited complex found in the wild type enzyme seems to be present, but not rate limiting, in the mutant Gln 143 Ala (Lévêque et al., 2000).

We have investigated position Gln 143 in human Mn-SOD with further amino-acid replacements to determine if we could (1) find the relationship, if any, between fast catalysis and product inhibition and (2) generate mutants at position 143 that would favor Mn^{3+} in the resting state. The crystal structure of the mutant containing the replacement of Gln 143 with Ala showed that two new water molecules were situated in positions nearly identical with the OЄ1 and NЄ2 of the replaced Gln 143 side chain (Figure 2-3). These water molecules maintained a hydrogen-bonded network in the active site cavity; however, their presence could not sustain the stability and activity of the enzyme. Each of the five replacements made at position 143 decreased catalytic activity two to three orders of magnitude compared with the activity of the wild type enzyme. In addition, mutants Gln 143 Ala and Gln 143 Asn each showed an optical spectrum during catalysis with an absorbance at 420 nm, which is evidence of a product inhibited complex (Bull et al., 1991; Hearn et al., 1999; Lévêque et al., 2000). Measurement of the decay of this absorbance suggests that the dissociation of the product-inhibited complex is not affected

by the replacement Gln 143 Ala. Hence, the features of the active site that influence catalysis appear to be different from the features that influence dissociation of the product-inhibited complex for these enzymes. This information is significant in designing mutants of Mn-SOD for gene therapy research that show less product inhibition than wild type and maintain a high level of catalytic activity.

Materials and Methods

Mutagenesis and Cloning

Transfer of the hMn-SOD cDNA from the phMnSOD4 clone to the pTrc 99A vector

The plasmid phMnSOD4 (ATCC #59947) contains the complete 222 amino acids (a.a.) human Mn-SOD precursor cDNA, in addition to a 5' and 3' untranslated region of 91 base pairs (b.p.) and 21 b.p., respectively. The first 24 a.a. of the Mn-SOD precursor constitute the signal peptide that is cleaved in mitochondria *in vivo* to give the mature 198 a.a. enzyme. For expression in bacteria, the cDNA encoding the mature enzyme plus the 3' untranslated region was amplified by polymerase chain reaction (PCR) using the phMnSOD4 clone as template and then ligated to the expression vector pTrc 99A. The two primers used for the reaction were, primer 1: 5'-C GCT AGT AAT CAT TTC ATG AAG CAC AGC CTC CCC G-3' which contains a BspH I restriction site followed by the cDNA sequence coding for the N-terminus of the mature protein. Primer 2: 5'-GCA GCT TAC TGT ATT CTG CAG-3' is identical to a 21 b.p. untranslated region downstream of the Mn-SOD gene. The PCR reaction was set up as follows: 2 ng of template, 250 mM dNTPs, 1.5 mM $MgCl_2$, 1 mM primers (1 and 2), PCR buffer (New England Biolabs), 1 unit of vent polymerase, and distilled H_2O to a final volume of 100 µl. The PCR reaction was run on an ERICOM thermocycler for 25 cycles with an annealing temperature of 65

°C. The PCR product (containing the human Mn-SOD cDNA plus a short 5' and 3' untranslated region) was purified by electroelution, digested with BspH I and Pst I, and ligated to the pTrc 99A vector. Before ligation, pTrc 99A was cut with Nco I (which has compatible ends with BspH I) and Pst I. The resulting clone (wild-type human Mn-SOD in pTrc 99A) was used as a template to generate specifically mutated Mn-SOD enzymes.

Generation of human Mn-SOD site-directed mutants

Deep Vent polymerase (New England Biolabs) was used to catalyze the PCR reaction. A series of primers were designed to create the mutants Q143X in human Mn-SOD (X=A,E,H,N,S,V). First, we designed a pair of oligonucleotides, primer 1 (5' - C GCT AGT AAT CAT TTC ATG AAG CAC AGC CTC CCC G - 3') and 2 (5' - CGC CAA AAC AGC CAA GCT TTC ATG CTC GCA G - 3'), which, through PCR, would recreate the entire Mn-SOD coding region. Second, we prepared two oligonucleotides for each mutant to be made, designated as primer 3 (5' - GCT GCT TGT CCA AAT CAG GAT CCA C - 3') and 4 (5' - G TGG ATC CTG ATT TGG ACA AGC AGC - 3'), whose sequences are complementary to each other and contain the mutation of interest at position 143 (underlined). Two separate PCR reactions were used to amplify the 5' half (primers 1 and 4) and 3' half (primers 3 and 2) of the Mn-SOD cDNA coding sequence. The PCR products from these two reactions were purified using electroelution and used as template DNA for the second round of PCR using primers 1 and 2 (figure 2-1).

The mutant gene obtained by the second round of PCR was then digested with Pst I and BspH I. The expression vector pTrc 99A was digested with Nco I (that has compatible ends with BspH I) and Pst I. The PCR product was then ligated into pTrc 99A and used for transformation in the *SodA⁻/SodB⁻ E. coli* strain QC774. Colonies are screened for positive clones by restriction digestion with Pst I and with the internal cut

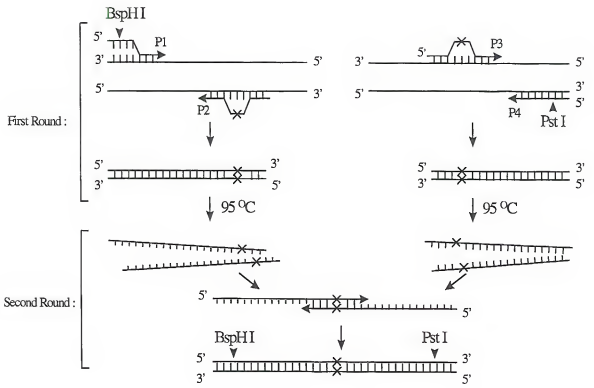


Figure 2-1: Scheme of the PCR reactions performed to generate point mutations in the Mn-SOD gene. "First round" corresponds to the first set of two PCR reactions that generate the two halves fragments. Those two fragments are used as a template for the "second round". P1, P2, P3, and P4 correspond to Primer 1, 2, 3, and 4, respectively. See text for details.

Sph I. One positive clone was then tested by a small scale protein production and sent to the sequencing core in order to check the exactitude of the entire DNA sequence. Both top and bottom strands were sequenced. Once the sequence was checked, the DNA clone was kept as a glycerol stock in QC774 cells at -80 °C, and as a plasmid DNA stock in TE buffer at -20 °C.

Bacterial Growth and Protein Expression

To produce each mutant enzyme, nine liters of bacterial culture were grown in rich yeast extract media (2 x YT) until OD_{600} = 0.4 - 0.5. At that point, cells were induced with 0.2 mM IPTG and 1 mM $MnCl_2$ was added to the culture. Four hours after induction, cells were harvested by centrifugation; pellets were recombined and frozen overnight at -80 °C. The mutant enzyme was then purified according to a modification of the procedure from Beck et al. (1988), as now described. The cell pellet was thawed and resuspended in 200 ml lysis buffer (40 mM KH_2PO_4, pH 7.8, 25% glycerol, 0.2 mg/ml lysozyme, 10 mm/ml DNase I, 0.1 mM EDTA, 400 µl/200 ml detergent Triton® x100, 1 mM PMSF). The cell extract was stirred for 30 minutes, passed twice through a French® pressure cell press (SLM Instruments, Inc.), heated at 65 °C for 40 minutes, and spun down. The supernatant was then dialyzed for 12 hours three times against 2 mM KH_2PO_4, pH 7.8, loaded on a DE-52 column (anion exchanger), washed with 200 ml of 2 mM KH_2PO_4 pH 7.8, and eluted with 20 mM KH_2PO_4, pH 7.8. Each 15 ml fraction was checked for enzyme by scanning spectrophotometry (from 210 nm to 310 nm) and fractions containing enzyme were recombined. The enzyme usually came out in 6 tubes but this number varied from one mutant to the next. The buffer (20 mM KH_2PO_4, pH 7.8) was then replaced by 20 mM potassium acetate (CH_3COOK) pH 5.5 by repeatedly concentrating the sample by ultrafiltration and diluting it back with the potassium acetate

buffer. The sample was then loaded on a CM-52 column (cation exchanger), washed with 20 mM potassium acetate, and eluted with a 20 to 200 mM potassium acetate gradient, pH 5.5. Fractions containing protein were identified by scanning spectrophotometry (same as above) and SDS-PAGE, recombined, and concentrated down to a volume of 3 to 30 ml by ultrafiltration. During this last step, the buffer was replaced by 2 mM potassium phosphate, pH 7.8. An additional SDS-PAGE gel was used to assess the purity of the protein. The yield achieved varied from one mutant to the next, but was typically around 70 mg of pure enzyme for 50 g of bacterial pellet. The pure enzyme was sterilized by filtration through a 0.22 mm syringe filter and kept sterile at 4 °C.

Crystallography of Q143A Mn-SOD

Crystallographic data were generated in collaboration with Dr. John A. Tainer at the Scripps Research Institute in La Jolla, California. The hexagonal crystals of Q143A Mn-SOD were grown out of 2.0 - 2.8 M ammonium sulfate and 100 mM imidazole / malate buffer at pH 7.5 or 8.0. The data were collected at the Stanford Synchrotron Radiation Laboratory from a single crystal that was frozen in its well solution containing 20% ethylene glycol. The structure was solved by molecular replacement using the AMoRe program from the hexagonal Y34F human Mn-SOD mutant (Guan et al., 1998) and the proper residues were changed using XFIT (McRee, 1999). The crystals were in space group p6(1)22 with a dimer in the asymmetric unit and the tetramer formed across a crystallographic two-fold axis. The unit cell was 79.6 Å x 79.6 Å x 241.6 Å with angles of 90°, 90°, and 120° for alpha, beta, and gamma, respectively. Based on the absorbance at 480 nm, the Mn was considered to be primarily reduced and was treated formally as Mn^{2+}. The Mn-bound solvent molecule was treated as a neutral water molecule.

Differential Scanning Calorimetry

A NANO high-sensitivity differential scanning calorimeter (Calorimetry Science Corp.) was used in collaboration with Dr. James R. Lepock (University of Waterloo, Canada) to obtain all denaturation profiles. Human Mn-SOD mutants were scanned at a concentration of 1.0 mg/ml in 20 mM potassium phosphate buffer (pH 7.8); samples were deaerated under mild vacuum for 5 min and immediately scanned at a rate of temperature increase of 1 °C/min. The baseline and change in specific heat (Cp) upon denaturation were corrected as previously described (Borgstahl et al., 1996). The peaks of the differential scanning calorimetry profile were fit assuming a reversible, non-two state model (Sturtevant, 1987) using the software package ORIGIN (Microcal, Inc.) to obtain the enthalpy (ΔH) and entropy (ΔS) values. The temperature of half-completion (T_m) for each transition was obtained from the integral for each curve.

Stopped-Flow Spectrophotometry

Kinetic data were generated using both a single wavelength and a diode array apparatus. Both instruments are described below.

Single wavelength apparatus

Experiments are based on the stabilization of potassium superoxide (KO_2) in aprotic solvent and the subsequent large dilution of this solution by an aqueous solution of enzyme in a stopped-flow apparatus (Kinetic Instruments, Ann Arbor, Michigan) as described by McClune and Fee (1976). KO_2 was dissolved in dimethyl sulfoxide (DMSO) with solubility of KO_2 enhanced with 18-crown-6 ether (Valentine and Curtis, 1975; McClune and Fee, 1978). The superoxide solution was kept in a desiccator and used the same day. Figure 2-2 shows a scheme of the stopped-flow apparatus. Syringe A (50 ml) was filled with enzyme, 50 mM EDTA, and buffer. Syringe B (1 ml) was filled

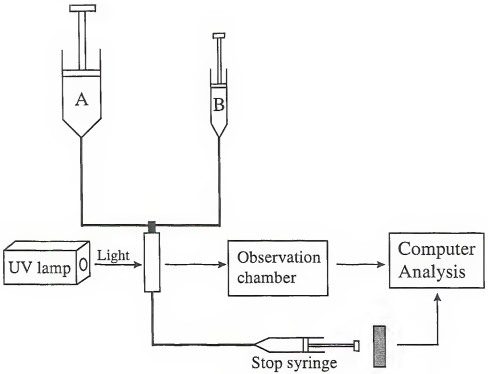


Figure 2-2: Schematic of the single wavelength stopped-flow apparatus. Syringe A (50 ml) is filled with buffer, enzyme, and EDTA. Syringe B (1 ml) is filled with the aprotic solution of superoxide. The "stop syringe" on the bottom stops the flow and triggers the computer to start data collection.

with the superoxide solution. The enzyme concentration varied with each experiment but was usually set around 3 to 5 μM. The variable parameter was either the pH of the reaction or the substrate concentration. The different buffers used for pH gradient studies were: MOPS (pKa 7.2) at pH 7.2 and 7.6, Glycylglycine (pKa 8.1) at pH 8.0, TAPS (pKa 8.2) at pH 8.4 and 8.8, CHES (pKa 9.2) at pH 9.2, and CAPS (pKa 10.1) at pH 10.0 And 10.6. The maximum superoxide concentration achievable by this method was about 800 μM and concentrations as low as 10 μM were obtained by diluting the initial aprotic solution with DMSO. Below 10 μM superoxide, the signal to noise ratio became too low for an accurate reading.

This stopped-flow apparatus was capable of efficient mixing of the contents of the two syringes (dead time between 1.5 and 2.0 ms), which then flowed into an observation cell while the previous contents were flushed and replaced with freshly mixed reactants. The stop syringe had a dual role: to limit the volume of solution expended by abruptly stopping the flow, and to simultaneously trigger the computer to start data collection. The reaction was followed by a spectrophotometer as the solution aged after the flow stopped. The decay of superoxide was monitored by its absorption at 250 nm. Eight traces were averaged to reduce noise. Steady-state parameters were obtained by least-squares analysis of the decay of superoxide ($\varepsilon_{250} = 2000\ M^{-1}cm^{-1}$) in both initial velocity experiments (the first 5% to 10% of reaction) and progress curves (Enzfitter, Biosoft, Cambridge, UK). Stopped-flow experiments reported here were carried out at 20 °C.

Diode array spectrophotometer

Experiments were performed using scanning stopped-flow spectrophotometry (SX18.MV; Applied Photophysics, Ltd., UK). We used a procedure of sequential mixing. First, a solution of potassium superoxide/crown ether in DMSO (described above) was

mixed at a 1:3.5 ratio with an aqueous solution of 2 mM Caps and 1 mM EDTA at pH 11. At this pH, superoxide is considerably stabilized (Marklund, 1976). This solution was aged one second and then mixed in a 1:1 ratio with an aqueous solution of 300 mM Ches at pH 9.0. Absorbance spectra after mixing were measured at a rate of 400 spectra per second.

Pulse Radiolysis

Experiments were carried out using the 2 MeV van de Graaff accelerator at Brookhaven National Laboratory, in collaboration with Dr. Diane E. Cabelli. All UV/Vis spectra were recorded on a Cary 210 spectrophotometer thermostated at 25° C. The path length was either 2.0 or 6.1 cm. Solutions contained enzyme, 30 mM sodium formate (as a hydroxyl radical scavenger (Schwarz, 1981)), 50 μM EDTA, and 2 mM of one of the following buffers: Mops (pH 7.2), Taps (pH 8.2), and Ches (pH 9.2). Superoxide radicals were generated upon pulse radiolysis of an aqueous, air saturated solution containing sodium formate according to the mechanisms described by Schwarz (1981). Under those experimental conditions, the formation of O_2 radicals is more than 90% complete by the first microsecond after the pulse. Changes in absorbance of superoxide or enzyme were observed spectrophotometrically.

Results

Structure and Spectroscopy.

The mutant Q143A human Mn-SOD had no significant change in overall structure compared with the wild-type enzyme; the root-mean-square deviation between Cα's of the mutant and the wild-type was 0.23 Å. However, the structure of the mutant

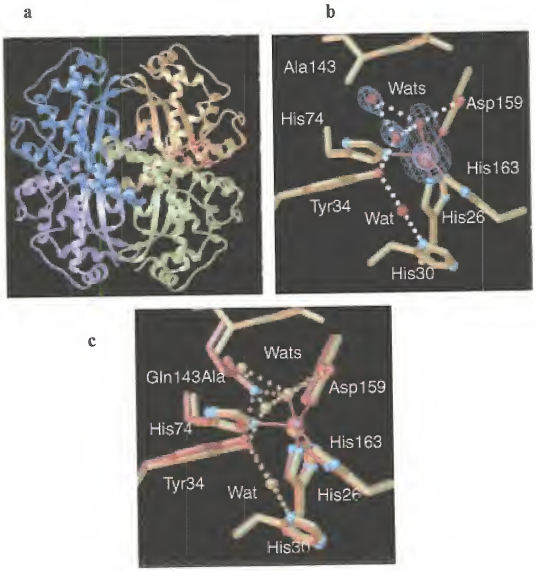


Figure 2-3: (a) The crystal structure of tetrameric human wild type Mn-SOD with subunits shown in different colors (Borgstahl et al., 1992). (b) The active site region from the crystal structure of the Q143A mutant. Solvent molecules are in the ball conformation (Wat). The hydrogen bonding network (white dots) includes the two solvent molecues (wats) not present in the wild type enzyme. (c) Superposition of the active-site regions from the crystal structures of the wild-type human Mn-SOD and the Q143A mutant. The residues from the wild-type Mn-SOD are pink and those from Q143A are gold.

shows that two new water molecules fill the cavity created by changing the glutamine to an alanine. Figure 2-3b shows that in Q143A, the new water molecules lie in nearly the same location as the NЄ and OЄ of the replaced Gln 143. In the wild type, an Mn-solvent-Gln143-Tyr34 structure has the OЄ1 or NЄ2 of Gln 143 connecting Tyr 34 to the Mn-bound solvent ligand. In Q143A, an Mn-solvent-H_2O-Tyr34 structure connects the Mn-bound solvent molecule to Tyr 34 (Figure 2-3b); thus, a novel water molecule restores the hydrogen bond scheme. The average Mn-solvent distance in Q143A Mn-SOD is about 2.25 Å, a distance that suggests a mixture of Mn^{3+} and Mn^{2+} with OH and H_2O ligands, respectively (Borgstahl et al., 1992). The other Mn-ligand geometries are typical of those for the wild-type human Mn-SOD enzyme.

Wild-type human Mn-SOD is purified predominantly in the Mn^{3+} state (Hsu et al., 1996) and exhibits a strong absorbance in the visible range with a maximum at 480 nm ($\varepsilon_{480} = 610\ M^{-1}cm^{-1}$). In contrast, the visible absorption spectra of the mutants at position 143 listed in Table 2-1 displayed only a very weak visible absorption ($\varepsilon_{480} < 30\ M^{-1}cm^{-1}$) characteristic of Mn-SOD in the Mn^{2+} state (typical spectra shown in Figure 2-4). This was taken as evidence that, like Q143N human Mn-SOD (Hsieh et al., 1998), these mutants have been purified with manganese predominantly in the reduced state. Moreover, the active sites of wild-type Mn-SOD were about 80-90% occupied by manganese and less than 3% occupied by iron whereas mutations at position 143 increased the iron content of the mutants as determined by atomic absorption spectroscopy. For example, Q143A Mn-SOD had 66% manganese and 10% iron. In samples of varied iron content, the catalytic activity correlated with the manganese

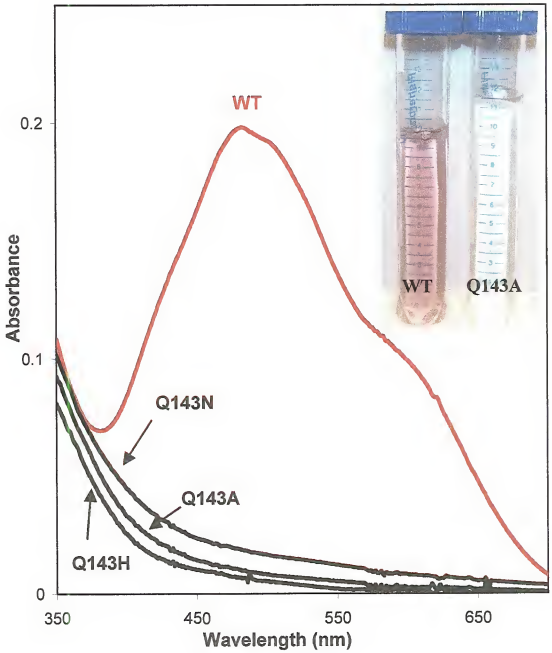


Figure 2-4: The visible absorbance spectra of wild-type human Mn-SOD and site-specific mutants Q143A, Q143H, and Q143N measured at pH 7.8 and 20 °C. Solutions contained 20 mM phosphate buffer and 100 μM EDTA.

content, indicating that the Fe-containing mutants were inactive or had activity too low to detect.

Catalysis

The catalyzed decay of superoxide was measured by stopped-flow spectrophotometry and pulse radiolysis from the absorbance of $O_2^{\cdot -}$ at 250 or 260 nm; Figure 2-5 shows typical data for Q143A Mn-SOD. Each of the mutants listed in Table 2-1 was adequately fit to Michaelis-Menten kinetics. Values of k_{cat}/K_m and k_{cat} were quite similar among mutants, and smaller than the values for wild-type Mn-SOD by two to three orders of magnitude (Table 2-1). Both k_{cat} and k_{cat}/K_m for these mutants showed no pH dependence in the pH range from 8.0 to 10.5; an exception was Q143N for which these parameters decreased with increasing pH (Hsieh et al., 1998). We also prepared and carried out measurements of the mutant Q143S; it had values of k_{cat} and k_{cat}/K_m that were too small to measure accurately because of the rapid competing uncatalyzed dismutation.

When observing the decreasing UV absorbance of superoxide (250 - 260 nm), catalysis by wild-type Mn-SOD exhibits a prominent zero-order phase in superoxide beginning about 2 ms after introduction of $O_2^{\cdot -}$ and characteristic of product inhibition (Hsu et al., 1996; Bull et al., 1991; McAdam et al., 1977a). When observing the absorbance of the enzyme itself, the product inhibited state of wild-type Mn-SOD has been associated with an absorbance at 420 nm ($\varepsilon_{420} = 500\ M^{-1}cm^{-1}$; Bull et al., 1991; Hearn et al., 1999). Both pulse radiolysis and scanning stopped-flow experiments with mutants at position 143 have detected such an absorption. In pulse radiolysis experiments, catalysis by Q143A Mn-SOD was accompanied by the emergence and decay of an absorbance at 420 nm (Figure 2-6). These data could be described by the sum

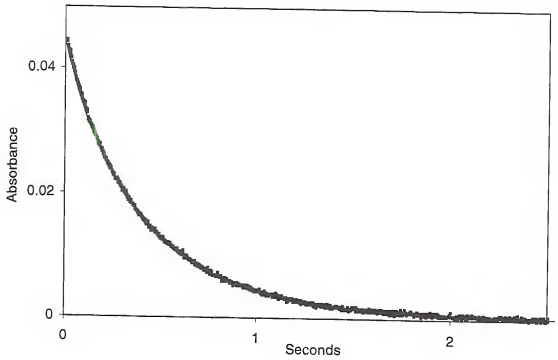


Figure 2-5: Superoxide decay catalyzed by Q143A Mn-SOD following introduction of superoxide by pulse radiolysis at 25 °C. Data show the decrease in absorbance at 260 nm due to superoxide ($\varepsilon = 2000\ M^{-1}cm^{-1}$, pathlength 2.0 cm; Rabani and Nielson, 1969). The initial concentration of superoxide was 22 μM and the solution contained 1.0 μM Q143A Mn-SOD, 2.0 mM Taps at pH 8.2, 30 mM sodium formate, and 50 μM EDTA. The solid line is a fit to a first-order decay giving a rate constant of $2.0 \pm 0.1\ s^{-1}$.

Table 2-1: Values of the pH-independent steady-state kinetic constants for the dismutation of superoxide catalyzed by wild-type human Mn-SOD and mutants at position 143.[a]

Residue at position 143	k_{cat} (ms^{-1})	k_{cat}/K_m ($\mu M^{-1}s^{-1}$)
Gln (wild type) [b]	40	800
Ala	0.50	3.1
Val [c]	0.8	0.7
Asn [b]	0.30	0.82
Glu	0.32	0.63
His	0.19	5.2

[a]Stopped-flow data collected at pH 9.6 and 20 °C, except where otherwise noted. The constants for these mutants were observed to be independent of pH in the range of pH 8.0 to 10.5 except for Q143N, which decreased with increasing pH (Hsieh et al., 1998). The standard errors were at most 15% for k_{cat}/K_m and 20% for k_{cat}.

[b]From Hsieh et al. (1998); data collected at pH 9.4 and 20 °C.

[c]Because the value of K_m for this mutant was near 1 mM, we were only able to roughly estimate K_{cat}. In this particular case, the estimated uncertainty is as great as 40%.

of two exponentials, one for the emergence and one for the decrease of the absorbance at 420 nm with rate constants given in the legend of Figure 2-6. These measurements were repeated at different wavelengths in the visible range, and the exponential decay was extrapolated to the initial time of mixing. The resulting plot (Figure 2-7) showed a maximum absorbance at 420 nm ($\epsilon_{420} = 160\ M^{-1}cm^{-1}$) and described a spectrum for the inhibited phase. Using scanning stopped-flow spectrophotometry and mixing maximum $O_2^{\cdot -}$ and Q143A Mn-SOD, we also observed spectra with a maximal absorption at 420 nm (data not shown).

Differential Scanning Calorimetry.

The thermal stabilities of the wild type and the position 143 mutants were determined by differential scanning calorimetry. In general, three melting temperatures can be observed for Mn-SOD (Borgstahl et al., 1996), a sometimes detectable but very weak transition labeled component A, a component B that is also very weak and corresponds to the thermal inactivation temperature of the wild type enzyme (Tm = 70 °C), and component C which is the main unfolding transition. The area of transition C is always greater than 95% of the total area of transitions A, B, and C. The five different residues incorporated at position 143 had profound effects on the heat stability of the enzyme (Table 2-2). In all cases, transitions A and B are barely detectable and were not observed for the mutant Q143S. This suggests that for Q143S, either transition B has a very small calorimetric enthalpy such that it is not detectable, or the two transitions B and C are superimposed. This was the case with the mutants at position 30 (Ramilo et al., 1999); an unambiguous identification of transitions A and B was not possible. However, the main unfolding transition C, which could be clearly measured, was the main determinant of conformational stability.

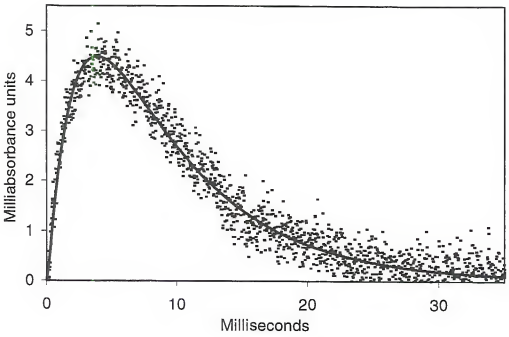


Figure 2-6: The emergence and decay of the absorbance at 420 nm (pathlength 2.0 cm) of Q143A Mn-SOD following the introduction of 13 μM superoxide by pulse radiolysis. The solution contained 90 μM Q143A Mn-SOD, 2.0 mM Taps, 30 mM formate, and 50 μM EDTA at pH 8.2 and 25 °C. The solid line is a fit to the sum of two exponentials giving rate constants of 447 ± 15 s^{-1} for the emergence and 125 ± 3 s^{-1} for the decay of absorbance.

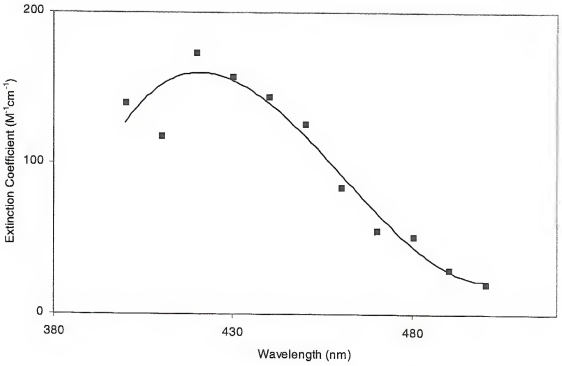


Figure 2-7: Change in extinction coefficient ε ($M^{-1}cm^{-1}$) as a function of wavelength obtained by extrapolation of the decreasing phase of absorbance to the initial time of mixing of superoxide and Q143A Mn-SOD. Data such as shown in Figure 2-6 were measured at a series of wavelengths; each set of data was fit to the sum of two exponentials, and the fit of the decay was extrapolated to time zero. Pulse radiolysis conditions were as described in Figure 2-6.

Table 2-2: Transition temperatures for the unfolding of wild type human Mn-SOD and mutants at position 143.

Residue at position 143	Tm (°C)
Glu	103.0
Ser	94.9
Asn[a]	90.7
Gln (wild type)[a]	88.9
His	88.9
Ala	79.8
Val	68.2

[a]From Guan et al. (1998).

Discussion

In the wild type Mn-SOD, Gln 143 participates in an extensive hydrogen-bonded network in the active site; it forms a hydrogen bond with the manganese-bound solvent and the phenolic hydroxyl of Tyr 34. Its replacement in Q143N (Hsieh et al., 1998) and Q143A (Figure 2-3) alters this hydrogen-bonded chain by inserting one or two water molecules, respectively, in this network. The more conservative replacements of Gln 143 with Asn and His had almost no effect on the main thermal unfolding transition Tm (Table 2-2); the values for Q143N (90.7 °C) and Q143H (88.9 °C) were similar to that of wild type (88.9 °C). The small effect on Tm of His 143 is interesting since His is found at this position in cambialistic bacterial Mn-SODs that can use manganese or iron interchangeably (Jackson and Cooper, 1998). Replacement of Gln with both Ala (79.8 °C) and Val (68.2 °C) significantly destabilized the enzyme, presumably because of the inability of these side chains to form hydrogen bonds, which in turn disrupted the hydrogen bonding network around position 143. In addition, Valine is the most destabilizing replacement and it is also the only replacement with a branched β-carbon. Replacement by Ser (94.9 °C) or Glu (103.0 °C) offered considerable stabilization, possibly because of a reinforcement of the hydrogen bonding network. We attempted to prepare Q143K, placing a positively charged residue at position 143; however, this mutant was too unstable to purify.

There is evidence that k_{cat} is determined at least in part by proton transfer processes that form product H_2O_2 in Mn-SOD (Bull et al., 1991) and Fe-SOD (Bull et al., 1985). This result extends to Q143N Mn-SOD for which the solvent hydrogen isotope effect on k_{cat} is 1.9 (Hsieh et al., 1998). The lower values of k_{cat} in catalysis by the site-

directed mutants of Table 2-1 compared with wild type suggest that, in spite of the presence of water molecules (that could potentially reform the hydrogen bonded network and provide a proton source and pathway), protons cannot be as efficiently transferred to the active site. The significance of the rather similar values of k_{cat} for the mutants of Table 2-1 suggests that there is considerable flexibility in the residues that can sustain k_{cat}, but none of them are able to participate in product formation to the same extent as in the wild-type Mn-SOD. The large decrease in the values of k_{cat}/K_m for the mutants of Table 2-1 compared with wild type most likely reflects changes in the redox potential at the metal. The visible absorption spectra (Figure 2-4) of selected mutants from Table 2-1 show that reduced metal is prominent, whereas in the wild type the oxidized metal predominates in the purified form in the resting state. In Q143A Mn-SOD, the appearance of water molecules at the approximate locations of the OЄ and NЄ of Gln 143 of wild type, and the formation of the hydrogen bonded network including these water molecules, was not sufficient to maintain either the catalytic activity or the redox potential of the mutant.

Hsieh et al. (1998) observed catalysis by human Q143N Mn-SOD and, based on the decay of the UV absorbance of superoxide, suggested no significant product inhibition. In fact, the observations in this report of the catalyzed decay of superoxide measured by the decrease of its UV absorbance are also consistent with no product inhibition; Figure 2-5 shows no evidence of a phase zero-order in superoxide during catalysis by Q143A Mn-SOD. However, during catalysis by these mutants we observed the presence of a transitory absorbance at 420 nm characteristic of product inhibition, shown for Q143A in Figures 2-6 and 2-7. The absorbance of Q143A Mn-SOD at 420 nm

gave an extinction coefficient near 160 $M^{-1}cm^{-1}$ when extrapolated to the time of introduction of superoxide (Figure 2-7), although this may not represent full inhibition of the enzyme. The estimated extinction coefficient of the product inhibited complex of wild-type Mn-SOD is near 500 $M^{-1}cm^{-1}$ (Bull et al., 1991; Hearn et al., 1999); wild-type Mn-SOD is more strongly product inhibited than Q143A, and hence this value is probably a more accurate estimate for the inhibited complex. Calculation shows that at the time of maximum absorbance of Q143A in Figure 2-6, approximately 5% to 15% of the active sites are in the product inhibited state, depending on which of the above extinction coefficients we use. Thus, although not detected as a deviation of first-order kinetics in Figure 2-5, there is a very small amount of product inhibition even in the mutant Q143A.

This allows us to comment on the characteristics of the product inhibited state by comparing the very weakly inhibited mutants of Mn-SOD in Table 2-1 with wild-type human Mn-SOD which exhibits considerable product inhibition (Hsu et al., 1996). The extent of inhibition is quantitated by the rate constant $k_o/[E_o]$ of the product inhibited phase of catalysis, which is zero order in superoxide (Hsu et al., 1996; Bull et al., 1991); values of $k_o/[E_o]$ are given in Table 2-3. Also included in this table is an estimate of the rate constants for the formation and dissociation of the product-inhibited enzymes (k_5 and k_{-5} of eq. 4) obtained from pulse radiolysis data such as shown in Figure 2-6. A rough estimate of these constants is obtained directly from the least-squares fit of these data to the sum of two exponentials which gives a value of k_5 of 5×10^6 $M^{-1}s^{-1}$ (dividing the rate constant for the emergence of the 420 nm absorption by enzyme concentration) and k_{-5} of 125 s^{-1}. These rate constants are a good approximation under the single turnover

Table 2-3: Values of the zero-order rate constant $k_o/[E_o]$ describing the product-inhibited phase, and rate constants k_5 and k_{-5} (of eq. 4) for the formation and dissociation of the product-inhibited complex, during the decay of superoxide catalyzed by human wild-type and Q143A Mn-SOD.

Enzyme	$k_o/[E_o]$ (s^{-1})	k_5 ($\mu M^{-1}s^{-1}$) [a]	k_{-5} (s^{-1}) [a]
Q143A	>2000 [b]	1.4	103 ± 10
Wild type	500	1,100	117 ± 5

[a] k_5 and k_{-5} of eq. 4 were determined by least-squares fit of the catalytic scheme of McAdam et al. (1977b) to the change in absorption at 420 nm; in this fit the values of the rate constants for the oxidation-reduction cycle of catalysis were made consistent with the experimentally observed values of k_{cat}/K_m.

[b] No zero-order region of enzyme inhibition was observed with this mutant. The lower limit was estimated from the smallest zero-order decay that would have been detectable in our measurements.

conditions of the pulse radiolysis experiments. A more refined estimate of the rate constant for k_5 and k_{-5} was determined from a least-squares fit of the rate constants of the McAdam mechanism of Mn-SOD (McAdam et al., 1977a) to a more extensive set of data which included the appearance and decay of the 420 nm absorbance (Figure 2-6), as well as the rate constants of the oxidation-reduction cycle. In this procedure, the rate constants describing the uninhibited oxidation and reduction cycles of catalysis were fixed at values consistent with the experimentally observed values of k_{cat}/K_m. This approach gave k_{-5} at $103 \pm 10\ s^{-1}$ for Q143A Mn-SOD in agreement with the former estimate. Similar measurements on the appearance and disappearance of absorption of wild-type human Mn-SOD following introduction of superoxide by pulse radiolysis (data not shown) gave a value of k_{-5} of $117\ s^{-1}$ (Table 2-3). This is comparable to the value of k_{-5} at $130\ s^{-1}$ for wild-type human Mn-SOD at 20 °C, estimated from the change in absorbance of superoxide during catalysis (Hsu et al., 1996) and to the value of $70\ s^{-1}$ by McAdam et al. (1977a) for *B. stearothermophilus* Mn-SOD at 25 °C. In contrast to these similar values of k_{-5} for Q143A and wild type, the values of k_5 differed by three orders of magnitude (Table 2-3).

The significance of the data of Table 2-3 is that even the very weakly active mutant Q143A shows evidence of product inhibition; moreover, the values of k_{-5} derived from the pulse radiolysis experiments are comparable in magnitude to those of the much more active and more inhibited wild-type Mn-SOD. Hence, Gln 143, which is necessary for maximal activity in superoxide dismutation, appears to have no role in the dissociation of the product inhibited complex. The identity of the product-inhibited complex has not been definitively described, but it is suggested to be a side-on peroxo

complex of Mn^{3+} at the active site (Bull et al., 1991). This complex would be expected to dissociate following proton transfer to form hydrogen peroxide. The results of Table 2-3 may indicate that proton transfer to this complex is similar in Q143A and in wild type Mn-SOD. The data also suggest that the dissociation of the product-inhibited complex described by k_{-5} is not affected by the change in redox potential for the mutants at position 143. The mechanism of McAdam et al. (1977a) and the more complex mechanism of Bull et al. (1991) for catalysis by Mn-SOD both show that the rate constant of the inhibited region that is zero-order in superoxide is proportional to the rate constant for the decay of the product inhibited state, k_{-5}, as well as dependent on other steps of the catalytic, oxidation-reduction cycle. Table 2-3 shows a net difference in the values of k_5 for wild type and mutant; however, this difference needs to be interpreted in terms of the greater differences in the other rate constants of the oxidation-reduction cycle. That is, the rate of appearance of inhibited complex will also depend on k_3 of eq. 1-7 which we have not determined. It is apparent that for Q143A Mn-SOD, the overall extent of product inhibition is less because the rate constants for the oxidation-reduction cycle (k_1 through k_4) and k_5 are less, not because the rate of dissociation of the inhibited complex is greater. These considerations will be significant in determining the properties of the product inhibition in human Mn-SOD and in the design of variants of Mn-SOD for gene therapy research, which are strongly catalytic but weakly inhibited.

CHAPTER 3
THE ROLE OF HISTIDINE 30

Introduction

Histidine 30 (His 30) is part of an extensive hydrogen-bonded network in Mn-SOD that extends throughout the active-site cavity involving side-chain residues, the aqueous ligand of manganese, and other water molecules, part of which is shown in Figure 3-1. The side-chain imidazole of His 30 forms two hydrogen bonds in human Mn-SOD; one with the side-chain hydroxyl of Tyr 34 through an intervening water molecule, and a second with the side-chain hydroxyl of Tyr 166 from the adjacent subunit in the dimer. This rather extensive hydrogen-bonded array could be involved in the proton transfer necessary to form product hydrogen peroxide by supporting a proton relay, or possibly some of these residues may be a source of the proton itself. Of course, the ultimate source of proton donation to product is from solution, and His 30, as well as Tyr 34, are partially exposed to solvent in human Mn-SOD. To investigate further the structural and functional role of His 30 in this hydrogen-bonded network in the active-site cavity of human Mn-SOD, I have prepared and measured catalysis of His 30 mutants, in collaboration with Dr. Cecilia A. Ramilo of our laboratory. Focus was placed on the potential role of His 30 in both fast catalysis and product inhibition. First, the crystal structure for the mutant containing the replacement His 30 Asn (H30N) was resolved in collaboration with Dr John A. Tainer, and showed that the mutation interrupts the hydrogen-bonded network in the active site. Second, calorimetric measurements were

performed and showed that the main unfolding transition was decreased by 12 °C in H30N, relative to the wild type enzyme. Third, the catalytic activity of this and other mutants at this site showed that His 30 is not essential for the catalysis, but its replacement caused substantial decreases in both k_{cat} and k_{cat}/K_m (about ten-fold). Since k_{cat} appears to have rate-contributing proton transfer steps in the wild type enzyme (Hsu et al., 1996), the decrease in k_{cat} caused by the replacements suggests decreased proton transfer in the maximum velocity of catalysis. The replacements at position 30 also caused a significant decrease in the extent of product inhibition compared with wild-type Mn-SOD.

Materials and Methods

Mutagenesis and Cloning

The cDNA encoding the mature human Mn-SOD enzyme plus the 3' untranslated region was used as template for PCR (for details see *materials and methods*, chapter 2). A series of primers were designed to create the mutants H30X in human Mn-SOD (X=A,E,K,N,Q,S). The pair of external nucleotides (primer 1 and 2) used for Gln 143 mutants (see figure 2-1) was also used here. Two oligonucleotides (primer 3 and 4) were used to introduce the mutation of interest at position 30 (underlined): primer 3 (5' CAG CTG CAC CAT TCG AAG CAC GCG GCC TA 3') and primer 4 (5' TAG GCC GC GTG GTG CTT CGA ATG GTG CAG CTG 3'). Those two primers also introduced a silent mutation to create a unique restriction site for later screening. PCR was performed as described in detail in chapter 2, under *materials and methods*. H30X human MnSOD PCR products were cloned into the expression vector pTrc 99A (Pharmacia Corp.). Mutations were verified by DNA sequencing, along with the remainder of the

coding sequence (both top and bottom strand). These constructs expressed human Mn-SOD as a mature protein in *E. coli* (strain QC 774). Culture conditions included 100 μM $MnCl_2$. Yields of human Mn-SOD mutant protein were close to the Gln 143 mutants and, on average, were 70 mg of protein per 50 g of bacterial pellet.

Bacterial Growth and Protein Expression

Mutants of human Mn-SOD were purified from *E. coli* according to the procedures of Beck et al.(1988) with the modification reported here in chapter 2, under *materials and methods*. The purity of the resulting samples was determined on SDS-PAGE which showed a unique intense band. Each mutant was analyzed for manganese content by atomic absorption spectrometry in order to determine the concentration of active enzyme on a monomeric basis. As in Gln 143 mutants, enzyme concentration was taken as the manganese concentration as determined by atomic absorption. Protein concentration was determined by the Lowry method and the fraction of active sites occupied by manganese was determined to vary from 0.68 for H30N Mn-SOD to 0.79 for H30A.

Crystallography of H30N Mn-SOD

Crystallographic data were generated in collaboration with Dr. John A. Tainer at the Scripps Research Institute in La Jolla, California. The mutant H30N crystallized from solutions consisting of 19.3 mg/ml protein buffered in 25 mM potassium phosphate at pH 7.8 and 20% polyethylene glycol (PEG) 2000 monomethyl ether. Rod shaped crystals were grown for two days and belonged to orthorhombic crystal form with unit cell dimensions of a=73.7Å, b=77.57 Å, and c=135.46 Å. One flash cooled H30N crystal was mounted under the liquid N2 stream and data collected at the Stanford Synchrotron Research Laboratory. The data were processed using DENZO (Otwinowski and Minor,

1997) and there were totally 35,154 unique reflections (99.9% complete). The structure of H30N mutant was solved with AMoRe (Navaza, 1994) using one dimer of human Mn-SOD as a search probe. His 30 in the native Mn-SOD structure was replaced with Asn using XFIT (McRee, 1992) and a tetrameric H30N mutant assembly was located in the asymmetric unit after rotation and translation search. The final model, consisting of four H30N subunits and 730 solvent molecules, was refined to 2.3 Å resolution.

Differential Scanning Calorimetry

These experiments were done in the laboratory of Dr. James R. Lepock, University of Waterloo, Canada. Two separate high-sensitivity differential scanning calorimeters were used to obtain all denaturation profiles (a Microcal-2 and a CSC NANO). Similar profiles were obtained from both calorimeters. Human Mn-SOD and mutants at a concentration of 1.0 mg/ml in 20 mM potassium phosphate buffer (pH 7.8) were deaerated under mild vacuum for 5 min and immediately scanned at a rate of temperature increase of 1 °C/min. The peaks of the differential scanning calorimetry profile were deconvoluted assuming a reversible, non-two state model (Sturtevant, 1987) using the software package ORIGIN (Microcal, Inc.). The temperature of half completion (Tm) for each transition was obtained from the best fits (Table 3-2).

Stopped-flow Spectrophotometry

Experiments are based on protocol developed by McClune and Fee (1978). For details and modifications see Chapter 2 *materials and methods*. Stopped-flow experiments reported here were carried out at 20 °C. Four or more kinetic traces were averaged to reduce noise. Steady-state parameters were obtained by both least-squares analysis of such data (Leatherbarrow, 1987) and analysis of progress curves (Bull et al., 1991).

Results

Structure of H30N Mn-SOD

Unlike the native and other functional mutant structures of Mn-SOD, which crystallize in space group $P2_12_12$ and have two Mn-SOD subunits in the asymmetric unit, H30N crystallized in space group $P2_12_12_1$ and had four Mn-SOD subunits in the asymmetric unit. Like the wild-type human Mn-SOD which is tetrameric (Hsu et al., 1996), the crystal structure of H30N is also tetrameric. The subunit fold and tetrameric assembly of the H30N mutant are very similar to the wild type with a root-mean-square deviation for Cα values of 0.56 Å. The superposition of the H30N tetramer and native tetramer shows a slight compression in the dimer interface region, and H30N has a more compact tetrameric association than the wild type.

The crystal structure of the mutant H30N Mn-SOD showed minimal changes in the orientation of residues in the active-site cavity, with Asn 30 having the same dihedral angle about the Cα-Cβ bond as His 30 in the wild-type enzyme (Figure 3-1). The primary structural changes in the H30N mutant involve altered local hydrogen bonds to solvent and side chains. In wild-type human Mn-SOD, a water molecule acts as a hydrogen-bonded bridge between the side chains of His 30 and Tyr 34 (Figure 3-1). Such a water molecule between Tyr 34 and Asn 30 also exists in the H30N mutant; however, it has lost its hydrogen bonding to the side chain at residue 30. Therefore, the Mn-solvent-Gln143-Tyr34-H_2O-His30-Tyr166 hydrogen-bonded relay, which is present in the wild-type enzyme, is broken in the H30N mutant (Figure 3-1).

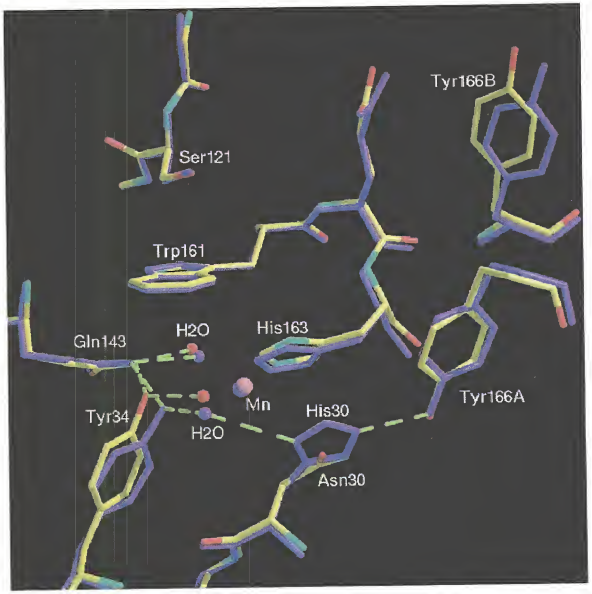


Figure 3-1: The least-squares superposition of the crystal structures of wild-type human Mn-SOD (blue) and H30N Mn-SOD (multicolored) showing residues in the active site. Asn 30 does not form a hydrogen bond to either the adjacent water molecule or the Tyr 166, and thus a hydrogen-bonded array in the active site is less extensive in the H30N mutant than in the wild type.

In wild type human Mn-SOD, Tyr 166 is hydrogen-bonded to the side chain of His 30 from the adjacent subunit of the dimer. In the H30N mutant, this bond is lost due to the shorter length and orientation of the side chain of Asn 30. Indeed, in the wild type, the phenolic OH of Tyr 166 forms a hydrogen bond to the Nϵ2 of His 30 (distance 2.8 Å); in the H30N mutant, the distance is 3.8 Å between the phenolic OH of Tyr 166 and the Oδ1 or Nδ2 of Asn 30, and therefore the hydrogen bond is lost. There is also an extensive hydrogen bond relay through water molecules in the dimer interface, which connects Gln 143 of subunit A to Val 160 of subunit B.

Catalytic Properties of His 30 Mutant Enzymes

Initial velocities of the decay of superoxide catalyzed by H30N Mn-SOD and measured by stopped-flow spectrophotometry could be fit to Michaelis-Menten kinetics. Typical rate data for H30N Mn-SOD are shown in Figure 3-2. The initial velocities of catalysis are calculated from the first 10% to 15% of the catalyzed decay, from which the uncatalyzed dismutation rates have been subtracted. The pH dependence of k_{cat}/K_m for superoxide decay catalyzed by H30N Mn-SOD can be roughly fit to a single ionization with an apparent pKa of 9.6 ± 0.1 (Figure 3-3). This pKa value is nearly the same as that for wild-type Mn-SOD. The maximal value of k_{cat}/K_m for H30N Mn-SOD was at pH 8.0 with a value near 2 x 10^8 $M^{-1}s^{-1}$, and about four-fold less than that for the wild-type enzyme (Figure 3-3). Conversely, the values of k_{cat}/K_m for the replacements His 30 Ala, Ser, and Gln had no apparent pH dependence in the range of pH 8 to 10.5, and are given in Table 3-1. For the replacements His 30 Glu and Lys, there was only very small catalytic activity (Table 3-1).

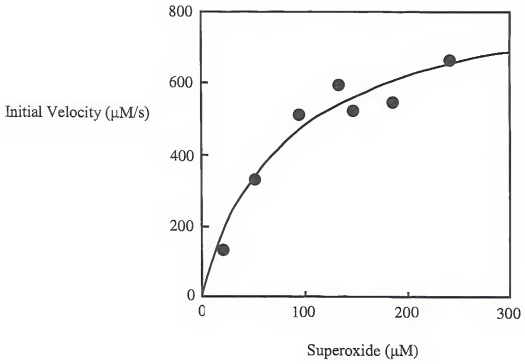


Figure 3-2: The initial velocities (μMs^{-1}) of the catalyzed decay of superoxide at 20 °C. Uncatalyzed rates have been subtracted. Solutions contained 10 mM Caps buffer at pH 10.0 and the concentration of H30N Mn-SOD was 0.25 μM. The solid line is a least squares fit of the data to the Michaelis-Menten equation with $k_{cat} = (5.3 \pm 0.7) \times 10^3\ s^{-1}$ and $k_{cat}/K_m = (6.6 \pm 1.4) \times 10^7\ M^{-1}s^{-1}$.

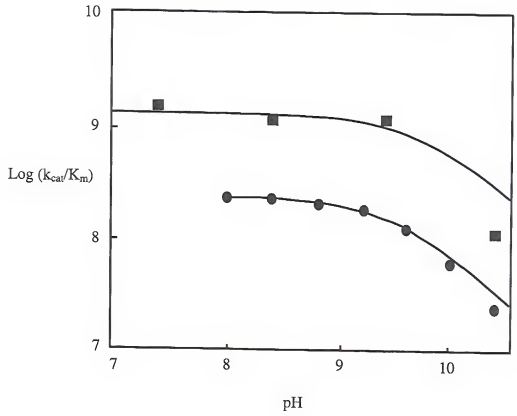


Figure 3-3: The logarithm of k_{cat}/K_m ($M^{-1}s^{-1}$) for the decay of superoxide catalyzed by wild-type human Mn-SOD (■); and H30N Mn-SOD (●) measured by stopped-flow at 20 °C. For H30N, the following buffers (10 mM) and pH's were used: glycylglycine (pH 8.0); Taps (8.4, 8.8); Ches (9.2) glycine (9.6), Caps (10.0, 10.4). All solutions contained 50 μM EDTA. The solid line for H30N Mn-SOD is a least-squares fit to a single titration with pKa 9.6 ± 0.1.

Table 3-1: Steady-state kinetic constants for the decay of superoxide catalyzed by human Mn-SOD and mutants at pH 9.4 or 9.6 and 20 °C [a].

Enzyme	k_{cat} (ms^{-1})	k_{cat}/K_m ($\mu M^{-1}s^{-1}$)
Wild Type [b]	40	800
Y34F [c]	3.3	870
H30N	4.3	130
H30A	2.4	61
H30S	2.3	63
H30Q	1.4	52
H30K [d]	1.7	1.6
H30E [d]	0.052	0.1

[a] Standard deviations for at least three measurements of k_{cat} were at most 15% and for k_{cat}/K_m were at most 20%.

[b] The value of k_{cat} for wild-type Mn-SOD was determined by numerical methods using data obtained by pulse radiolysis (Hsu et al., 1996).

[c] From Guan et al. (1998)

[d] These data at pH 9.4, the others at pH 9.6

The values of k_{cat} (Table 3-1) for the mutants H30N, Q, S, and A were all independent of pH (from pH 8.0 to 10.5). Those values were decreased by approximately 10- to 40-fold compared to wild type (Table 3-1), with the exception of H30E. The value for wild type ($k_{cat} = 40\ ms^{-1}$) was obtained by a computer fit of pulse radiolysis data (Hsu et al., 1996). The most active mutant, H30N, had a value of k_{cat} 10 fold less compared to wild type (Table 3-1).

The solvent hydrogen isotope effects on the steady-state constants were determined for catalysis by H30N Mn-SOD in solutions containing 10 mM glycine buffer at pH 9.4 (uncorrected pH meter reading) and 20 °C. The ratio of k_{cat} measured in H_2O with that in D_2O (0.98 atom fraction D) was $Dk_{cat} = 2.1 \pm 0.1$. The corresponding solvent hydrogen isotope effect on k_{cat}/K_m was $Dk_{cat}/K_m = 1.2 \pm 0.4$.

Another change, caused by the replacements His 30 Ala, Asn, and Gln is that the resulting mutants show less product inhibition in their catalysis of superoxide dismutation than does wild type. Product inhibition in Mn-SOD is characterized by a region of zero-order decay of superoxide, and is prominent in both wild type (Hsu et al., 1996; Bull et al., 1991) and Y34F Mn-SOD (Guan et al., 1998). It is not clear why product inhibition is less in the position 30 mutants, but probably part of this absence is due to the slower catalytic activity of the mutants. That is, there is less product inhibition when the rate of product formation is lower. Other factors may enter, however, such as the effect of His 30 on the stability of the enzyme-peroxide complex.

Thermal Stability

The thermal stability of the mutants with replacements at position 30 was determined by differential scanning calorimetry and was compared with the stability of the wild-type human Mn-SOD (Table 3-2). For the wild-type enzyme, two prominent

transitions have been observed (Borgstahl et al., 1996); transition C is the main unfolding transition at 89.9 °C (Tm), and transition B (at 70 °C) corresponds to the thermal inactivation temperature, from which the theoretical half-life of the enzyme can be calculated (Borgstahl, 1996). None of the mutants at position 30 have a transition that can be clearly associated with the inactivation transition B. Only transition C, the main unfolding transition, is resolvable. This suggests that either the two transitions have been superimposed for the mutants or that the inactivation transition B has such a small calorimetric enthalpy for the mutants that it is not detectable. However, the main unfolding transition C, which can be determined unambiguously, is the determinant of conformational stability.

Table 3-2: Main unfolding transitions (Tm) for the reversible unfolding of native human Mn-SOD and mutants at position 30.

Enzyme	Tm (°C)
Wild Type	89.9
H30Q	80.4
H30N	78.2
H30S	75.4
H30A	74.1

In 20 mM potassium phosphate, pH 7.8, the Tm (transition C) for wild type Mn-SOD is 89.9 ± 1.1°C, and the Tm's for the mutants range from 74° to 80° C (Table 3-2). This indicates that the conformational stability of the mutants is considerably less than wild type.

Discussion

In wild-type human Mn-SOD, a hydrogen-bonded chain extends from the aqueous ligand of the manganese to the side chain of Tyr 34 and then through a hydrogen-bonded water to the His 30 side chain, which in turn is hydrogen-bonded to the phenolic hydroxyl of Tyr 166. In addition the side chain of His 30 is partially exposed to bulk solvent. However, in H30N Mn-SOD, the side chain of Asn 30 does not appear hydrogen bonded to the corresponding water molecule nor to Tyr 166 (Figure 3-1). Therefore, a hydrogen-bonded array involving residue 30, which may be involved in the protonation of product peroxide, is not as extensive in H30N as it is in wild type.

The main unfolding transition measured by differential scanning calorimetry for the mutants at position 30 listed in Table 3-2 decreased by 10 to 16°C compared with wild type. It is interesting that the result for the mutant of human Mn-SOD containing the replacement Y34F enhanced stability of this transition by nearly 7 °C (Guan et al., 1998). Both replacements H30N and Y34F caused apparent breaks in the hydrogen-bond network in the active site. Hence, the effect of these replacements are more complex than assigning them only to the break in the hydrogen-bonding network. Of relevance is the mutation Q143N, which stabilizes Tm by 1.8 °C (Hsieh et al., 1998). Y34F and Q143N are in close proximity, and both mutations cause similar reductions in molecular volume equivalent to one O and one CH2, respectively. Thus, this region may be under some strain, which is reduced by the Y34F and Q143N substitutions resulting in increased protein stability.

The overall effect of the replacement of His 30 by other residues is to substantially reduce both k_{cat} and k_{cat}/K_m (Table 3-1). Indeed, both k_{cat} and k_{cat}/K_m for the

catalysis of superoxide dismutation decreased by approximately an order of magnitude upon replacing His 30 with Asn in human Mn-SOD (Table 3-1). Thus, His 30 is not essential for catalysis. This conclusion was also reached for H30A Mn-SOD from *Saccharomyces cerevisiae* by Borders et al. (1998), although their results using a pyrogallol autooxidation assay determined that catalytic activity in this mutant was approximately unchanged compared to wild type.

It is interesting to notice that the conservative mutations H30N and Y34F, which interrupt the hydrogen-bonded array of side chains and water molecules in the active-site cavity, appear to have about the same effect on the maximal turnover number k_{cat} (Table 3-1). There was about a 10-fold decrease in k_{cat} compared with wild type with several different side chains placed at residue 30 (Ala, Asn, Gln, Lys, Ser). Since proton transfer events appear to be rate contributing for k_{cat}, we interpreted changes in k_{cat} upon these replacements in part as effects on intramolecular proton transfer (although there may be effects on other steps of the catalysis as well). The fact that conservative substitutions at residues 30 reduce k_{cat} for Mn-SOD by about an order of magnitude may signify that we have reduced the effectiveness of the proton delivery network of the wild type by each of these mutations. This is perhaps another manifestation of the hydrogen-bond network observed in the crystal structure and with the ionization of Tyr 34 in Fe^{2+}-SOD, which affects the NMR chemical shifts of many active site residues (Sorkin et al., 1997). Moreover, the observation that many mutations at position 30 result in about the same reduced value of k_{cat} compared with wild type, may signify that no residue we have used to replace His 30 participates in a proton transfer network that is as effective in catalysis as the network in the wild type. The observation that the mutant H30K gives k_{cat}

comparable to Ala or Asn demonstrates that residue 30 can be positively charged, as well as His 30, with retention of considerable activity. Glutamate at position 30 results in a decrease in k_{cat} by about three orders of magnitude; this site cannot achieve effective catalysis with this negatively charged residue, a result perhaps due in part to repulsion of the superoxide radical anion.

For the wild type Mn-SOD, k_{cat}/K_m at 8 x 10^8 $M^{-1}s^{-1}$ is very near encounter controlled. The six-fold lower value for the mutant H30N indicates a change in rate-limiting step, in the sense that diffusion is less limiting. The pH profile for k_{cat}/K_m for H30N retains some pH dependence indicating a group with pKa near 9, as does the wild type (Ramilo et al., 1999). This is possibly the pKa for hydroxide binding as in E. coli Mn^{3+}-SOD (Whittaker et al., 1997) or possibly Tyr 34 as seen in E. coli Fe^{2+}-SOD (Sorkin et al., 1997), although it does not affect k_{cat}. The other mutants with replacements His 30 Ala, Gln, and Ser showed no apparent pH dependence in k_{cat}/K_m; this is the only significant kinetic difference we have observed among the mutants containing Ala, Asn, Gln, and Ser at position 30.

CHAPTER 4
REDOX PROPERTIES OF HUMAN MANGANESE SUPEROXIDE DISMUTASE

Introduction

A key element in catalysis by superoxide dismutases, is the successful transfer of electrons between the metal center of the enzyme and superoxide. The thermodynamic spontaneity of an electron transfer can be calculated knowing the standard midpoint potential (E_m) of the enzyme and comparing it with the known E_m of each redox couple involved in the dismutation of $O_2^{\cdot -}$ (eq. 4-3 and 4-5). E_m is an intrinsic parameter of the redox couple and reflects the relative stability of the two oxidation states. The Nernst equation (eq. 4-1) provides a quantitative relationship between the midpoint potential E_m and the ratio of the concentrations of the redox couple (eq. 4-2). E_h denotes the ambient potential referenced to the standard hydrogen half cell, also writen as E versus normal hydrogen electrode (or NHE). Both the solvent and ligand environment of the metal affect this relationship.

$$E_h = E_m + \frac{RT}{nF}\ln\frac{[ox]}{[red]} \qquad (4\text{-}1)$$

$$ox + ne^- \rightleftarrows red \qquad (4\text{-}2)$$

Superoxide dismutases have midpoint potentials that lie between +200mV and +400mV at pH 7 and are optimized to efficiently catalyze both reactions of $O_2^{\cdot -}$ dismutation (see eq. 1-6 and 1-7; Vance and Miller, 1998a; Azab et al., 1992; St.Claire et al., 1991; Barrette et al., 1983; Lawrence and Sawyer, 1979). The potential of free

manganese in solution ($Mn^{2+/3+}$) is 1510 mV, and that of $Fe^{2+/3+}$ is 770 mV (for review see Sawyer et al., 1995). Therefore, SODs tune the midpoint potential of their respective ligated metals to optimize electron transfer during both reactions of superoxide dismutation (eq. 1-6 and 1-7). In general, Mn-SODs must depress the E_m of $Mn^{2+/3+}$ by 1000 to 1300 mV, relative to the free metal potential in aqueous solution, for the E_m to lie half way between the two redox couples involved in the catalytic dismutation (eq. 4-3 and 4-5).

$$O_2^{\cdot -} \rightleftarrows O_2 + e^- \qquad E_m = -160 \text{ mV} \qquad (4\text{-}3)$$

$$Mn^{2+}SOD \rightleftarrows Mn^{3+}SOD + e^- \qquad -160 \text{ mV} < E_m < +890 \text{ mV} \qquad (4\text{-}4)$$

$$H_2O_2 \rightleftarrows O_2^{\cdot -} + 2H^+ + e^- \qquad E_m = +890 \text{ mV} \qquad (4\text{-}5)$$

Optimal catalytic activity requires optimization of all steps in the mechanism. Since Mn-SOD acts alternatively as an oxidant (eq. 4-3 and 4-4) and a reductant (eq. 4-4 and 4-5) during the disproportionation of superoxide, efficient catalysis is achieved when the midpoint potential of the enzyme is about half way between the respective potentials of the couples $O_2^{\cdot -}$ / O_2 and $O_2^{\cdot -}$ / H_2O_2. Since the catalytic rate of $O_2^{\cdot -}$ disproportionation by human Mn-SOD is close to diffusion controlled under non-inhibiting conditions (Hsu et al., 1996), it is anticipated that the midpoint potential of this enzyme should be around 350 mV.

The Need for Mediators

Superoxide dismutases have not evolved as electron transporters. Thus, even though electron transfer steps do occur between the metal redox center of the enzyme and the substrate superoxide, the chemistry of the reaction is buried in the active site, about 18 Å away from the surface of the protein. This fundamental difference between SODs

and electron carriers (like cytochrome c) has a profound effect on the study of their redox properties and complicates greatly the measurements made on SOD enzymes. The distance that separates the metal center of Fe- and Mn-SODs from the surface of the electrode prevents direct electron transfer from one to the other. Experiments reported here and elsewhere (Barrette et al., 1983; Verhagen et al., 1995; Vance, 1999) demonstrate that oxidative or reductive titrations of Mn-SOD alone give random potential values that do not correlate with the oxidation state of the enzyme (calculated from spectral data). This prohibitive distance requires the presence of an "electron bridge" to transfer electrons between the two entities. This electron bridge, or small molecule, is called a mediator.

Finding an appropriate mediator became one of the most difficult aspects of determining the redox potential of human Mn-SOD. Although thousands of mediators are commercially available, the set of conditions required for successful mediation narrowed to two the number of appropriate mediators among 15 tested; those are ferricyanide, $Fe(CN)_6$, and pentacyanoaminoferrate, $Fe(CN)_5NH_3$. The conditions for successful mediation were empirically established, and are described later in this Chapter. The use of two distinct mediators with different midpoint potentials and spectral signatures was necessary to rule out the possibility of measuring the redox potential of the mediator itself when mixed with the enzyme (or of a mediator/enzyme complex).

Determining the Extinction Coefficient of Human Mn-SOD

Among the landmarks that need to be established before a potentiometric titration may begin is determining the extinction coefficient (ε) of the enzyme and of each mediator and titrant to be used. Finding an accurate extinction coefficient for human Mn-SOD was challenging. Whittaker (1991) established the value of 850 $M^{-1}cm^{-1}$ for the

extinction coefficient of *E.coli* Mn-SOD using octomolibdocyanide [$Mo(CN)_8$] and hexachloroiridate ($IrCl_6$) as oxidizing agents. However, those chemicals have rather high midpoint potentials (eq. 4-6 and 4-7) and have a tendency to degrade the enzyme, which complicates the deconvolution of the data and the calculation of an accurate extinction coefficient (Whittaker, 1991).

$$Mo^{V}(CN)_8^{3-} + e^- \leftrightarrow Mo^{IV}(CN)_8^{4-} \qquad E_m = +800mV \qquad (4\text{-}6)$$

$$Ir^{IV}Cl_6^{2-} + e^- \leftrightarrow Ir^{III}Cl_6^{3-} \qquad E_m = +1020mV \qquad (4\text{-}7)$$

An extinction coefficient of 525 $M^{-1}cm^{-1}$ at 480 nm for human Mn-SOD has previously been reported (Hsu et al., 1996). This value was refined in this study for two reasons: (1) the accuracy of the value used for the extinction coefficient of the enzyme has a profound effect on the validity of the data, and (2) this value is sensitive to the environment of the enzyme (Dutton, 1978) and had to be determined under our experimental conditions (100mM KH_2PO_4/100mM KCl pH 7.8).

In order to measure the extinction coefficient of human Mn-SOD, I used potassium permanganate as the oxidizing agent to generate 100% oxidized enzyme. Potassium permanganate ($KMnO_4$, eq. 4-8) has a lower E_m than $Mo(CN)_8$ and $IrCl_6$, but is still high enough to oxidize the enzyme efficiently. In addition, $KMnO_4$ does not interact with (nor degrade) Mn-SOD. However, $KMnO_4$ has its own limitations; the

$$Mn^{VII}O_4^- + e^- \leftrightarrow Mn^{VI}O_4^{2-} \qquad E_m = +560mV \qquad (4\text{-}8)$$

formation of a solid manganese oxide complex (MnO_2). This complex forms in a pH dependant manner (4-9) and was observed experimentally at pH 7.8. Although the

$$Mn^{VII}O_4^- + 2H_2O + 3e^- \leftrightarrow Mn^{IV}O_2(s) + 4OH^- \qquad E_m = +600mV \quad (4\text{-}9)$$

absorbance of manganese oxide complicated spectral data, its formation was relatively

slow compared to the rate of oxidation of the enzyme by permanganate and did not prevent an accurate measurement of the extinction coefficient of the enzyme at 480 nm.

Measuring the Redox Potential of Human Mn-SOD

Two different approaches are available to measure redox potentials: electrochemical and coulometric titrations. Coulometric experiments have been done on membrane bound enzymes and purified enzymes (Hawkridge and Kuwana, 1973; Stankovich, 1980). In this technique, fully oxidized enzyme is gradually reduced as an electric current adds electrons to the system. The advantage of this technique over electrochemical titration is that, with purified enzyme, quantitative information can be derived (in the micromolar range) about the concentration of redox groups present (Stankovich, 1980). As a consequence, the extinction coefficient (ε) of all species in solution (enzyme and mediator) can be derived from the ratio of the difference in absorbance versus the difference in current. In addition, the number of electrons (n, see eq.4-1) transferred to the system is directly obtainable. Conversely, those two parameters can only be indirectly obtained by electrochemical titration.

Electrochemical methods have been extensively applied to enzymes that are part of electron transport systems (Wilson, 1978). However, a growing literature reports the application of this technique to other enzymes where electron transfer is just part of the catalytic process. (Barman and Tollin, 1972; Swartz and Wilson, 1971; Hendler and Shrager, 1979; Watt, 1979; Vance and Miller, 1998b). Most measurements are based on the change in absorbance (ΔA) as a function of the change in potential (ΔE). For systems where only one electron is transferred at a time (as it is the case with Mn-SOD), E represents the potential of the system at equilibrium, and $\Delta A/A$ (where A is the absorbance at t=0) is directly correlated to the total change in concentration of one

member of the redox couple. This is not true for more complicated systems where more than one electron is transferred at a time.

In the present study, the coulometric technique was used in collaboration with Dr. Kirk S. Schanze (Department of Chemistry, University of Florida) for the prescreening of potential mediators, but not for determining the midpoint potential of the enzyme itself. Instead, my focus was placed on setting up and using the necessary equipment to perform electrochemical titrations. In addition, work done by other groups (Vance, 1999) showed that coulometric titration of *E.coli* Mn-SOD using cyclic voltametry was fairly limited and complex because of the low stability of the bacterial enzyme in the presence of a relatively strong electric current. This observation emphasizes the fact that SODs have not evolved as electron transporters and do not "cooperate" with electron transfer measurements.

Materials and Methods

Gene Cloning and Protein Expression

Human Mn-SOD was cloned and overexpressed in *E.coli* (Hsu et al., 1996) using a modification of the protocol from Beck et al., 1988 (for details see Chapter 2, *Materials and Methods*). The construct expressed human Mn-SOD in the *E.coli* strain QC 774 (*sod A*$^{-}$*/B*$^{-}$) as a mature protein tagged with an extra methionine at the amino terminus. Culture conditions included either 100 μM $MnCl_2$ (for M9 media) or 1 mM $MnCl_2$ (for 2xYT media). Protein yields were on average 70 mg of protein per 50 g of bacterial pellet. Purity of the enzyme was determined on SDS-PAGE, which showed one intense band.

Metal Analysis

Every batch of pure enzyme was extensively dialyzed against EDTA in deionized water to remove metals (mainly Mn and Fe) not strongly bound to the enzyme. Experimentally, we found that dialyzing the enzyme more than 3 times for 12 hours did not lower any further the amount of total manganese content. Enzyme was run through a desalting column (P-10, Pharmacia) to remove the metal-EDTA complexes. Atomic absorption spectroscopy was used to measure the total manganese content in each batch of enzyme. A calibration curve with standard solutions was generated before each use. The protein concentration was determined using the Lowry assay and compared to the metal content to calculate the manganese content per monomer of enzyme.

Potentiometric Measurements of Human Mn-SOD

Instrumentation

Following a visit to the laboratory of Dr. Anne-Frances Miller (Johns Hopkins University, Baltimore) in June 1998, I designed, ordered, and installed the appropriate equipment to perform redox potential measurements in our laboratory. The equipment consists of a computer controlled diode-array spectrophotometer (Hewlett Packard 8453), a custom made anaerobic cell, and a computer controlled combination electrode (Microelectrodes, Inc.). Potentiometric titrations were performed at 25 °C in an anaerobic cell engineered in our laboratory (Figure 4-1). The design of this cell was based on the optical cell described by Stankovich (1980). The combination electrode (Ag/AgCl and Pt) was inserted in the main port of the cell while the first auxiliary port was used to degas the cell's chamber and introduce purified nitrogen (N_2). Oxygen was excluded from the nitrogen line via a trap filled with methyl viologen reduced with dithionite in water. A secondary vacuum trap was used to retain any excess methyl viologen in case of back

flow, and a filter (filled with indicating desiccant) was used to retain any humidity from the N_2 before reaching the cell. A second auxiliary port was used to add mediators, oxidizing and reducing agents, and to monitor enzyme concentration. During experiments, an air-propelled plate located under the spectrophotometer continually stirred the cell.

Mediators

A series of rules were empirically developed to pick appropriate mediators from the numerous chemicals commercially available. The mediator had to be soluble in water and not interact with nor precipitate the buffer used in the titrations. It also had to be small enough to fit into the active site cavity and have an intrinsic redox potential (E_m) near that of the enzyme (initially estimated at 350 mV). Ideally, the mediator should have signature peaks of absorbance in the visible range but not near that of the enzyme (450 to 600 nm). This last condition was not required but desirable to enhance the amount of data retrievable from the absorbance spectra of the enzyme with the mediator. All these requirements were necessary but not always sufficient to observe interaction between the mediator and the enzyme.

Potential mediators that satisfied all these conditions were titrated to check their intrinsic midpoint potentials and relevant extinction coefficient(s) at signature peak(s) of absorbance. Of all the chemicals tested (table 4-1), only two - ferricyanide $Fe(CN)_6$ and pentacyanoaminoferrate $Fe(CN)_5NH_3$ - were effective for titrations of human Mn-SOD (Table 4-2). In addition, these two mediators equilibrated slowly with the enzyme and reached equilibrium after up to 35 hours (depending on their relative oxidation state with the enzyme). Because such long periods of time were required to achieve equilibrium, oxidative and reductive titrations were extremely hard to perform and complicated by

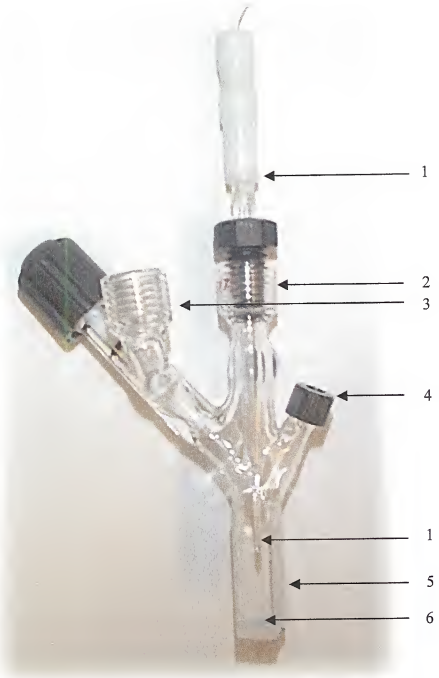


Figure 4-1: Anaerobic cell engineered in our laboratory for all potentiometric measurements. The main parts are the combination electrode (1), the electrode port (2), the vaccuum/N_2 port (3), the mediator/titrant port (4), and the 3 ml Pyrex cuvette (5). Solution was constantly stirred by a mini stir bar (6).

enzyme degradation. As a consequence, single point experiments (where enzyme and mediator were allowed to equilibrate in the absence of a titrating agent) were favored over potentiometric titration.

Cyclic voltametry was attempted to measure E_m of potential mediators as well as the reversibility of their redox couple under the required conditions. Some mediators did not exchange electrons with the electrode surface efficiently, and small amplitudes were seen in both the anodic and cathodic waves. In addition, waves were very noisy. Co-EDTA is a good example of a poor candidate for cyclic voltametry and, interestingly, did not interact with the enzyme either. Conversely, ferricyanide is known to be one of the best reversible couples according to cyclic voltametry (Vance, 1999) and was also the best mediator for human Mn-SOD.

Single point experiments

Possible mediators for the redox titration of human Mn-SOD were tested by single point experiments in which mediator and enzyme were allowed to equilibrate from opposite redox states. Three milliliters of pure enzyme (at 0.5 to 1 mM concentration of monomers in 100 mM phosphate buffer/100mM KCl pH 7.8) was introduced to the anaerobic cell and a spectrum of absorbance was taken as a reference point. The cell was then supplemented with an appropriate amount of mediator (enzyme:mediator from 1:1 to 1:10), sealed with the combination electrode, and degassed. The approach to equilibrium was monitored by two methods: optically, by using absorbance spectra of the enzyme between 400 to 700 nm (and also of the mediator at known optical signature(s)), and electrochemically by using the potential recorded by the electrode. Equilibrium was considered attained when the rate of change of the potential with time fell below 1 mV per 20 minutes (drift due to oxygen leakage into the system). The enzyme concentration

was checked (ϵ_{280} = 40,500 $M^{-1}cm^{-1}$) before and after each experiment. The fraction of enzyme in the oxidized state was determined from the optical absorbance at 480 nm (ϵ_{480} = 600 $M^{-1}cm^{-1}$), from which was deducted the absorbance of the enzyme in the reduced state (ϵ_{480} = 50 $M^{-1}cm^{-1}$). The percent oxidation of the mediator at equilibrium was also calculated from the optical spectra. The percent oxidation of the enzyme was plotted versus the ambient potential (E_h) and E_m was determined from the Nernst equation (eq. 4-10) assuming a single electron transfer per active enzyme monomer.

$$E_h = E_m + 59.2 \log (ox/red), \qquad (4\text{-}10)$$

where E_h is the measured ambient potential at equilibrium in millivolts (mV), E_m is the midpoint potential obtained from the equation (in mV), ox/red is the ratio of oxidized to reduced enzyme at equilibrium, and 59.2 = 2.303 x RT/nF where n=1. The standard errors in E_m calculated from the fits are given in the Results section and are typically in the range of 10 to 30 mV.

Redox titration

Ferricyanide was used as a mediator for the reductive titration of human Mn-SOD with dithionite, in the same anaerobic cell as described above. Three milliliters of oxidized Mn-SOD at 0.8 to 1mM monomeric concentration was mixed with $Fe(CN)_6$ with an excess of enzyme of 10:1, and degassed. Human Mn-SOD was titrated by adding 10% aliquots of dithionite as a reducing agent. At each addition of titrant, the system was allowed to equilibrate for 1 to 8 hours, depending on the rate of potential change. Titration was completed when the enzyme was 100% reduced and the potential dropped bellow 200mV (versus NHE). Oxidative titration with permanganate was attempted but the equilibration rate between enzyme and mediator was too slow to allow accurate reading of the potential during reoxidation of the enzyme. As a consequence, the

oxidative process was complicated by enzyme degradation and the data could not be fit to the Nernst equation.

Results

Extinction Coefficient of Human Mn-SOD and Mediators

The extinction coefficient of fully oxidized Mn-SOD was calculated and used as a reference for the deconvolution of the redox titration data (see below). The accuracy of the measurement depends on two factors; (1) the manganese to protein ratio (percent of sites occupied by manganese), and (2) the oxidation state of the manganese. The metal occupancy, determined by atomic absorption spectroscopy was around 90% ± 5% and varied slightly from one batch of enzyme to the next. The oxidation state of newly purified batches of enzyme was around 90% oxidized. This value was back calculated from the absorbance of fully oxidized enzyme (see figure 4-3).

Potassium permanganate ($KMnO_4$) was used to obtain 100% Mn^{3+}-SOD. This oxidizing agent did not show any binding affinity with the enzyme based on its absorbance spectra. However, manganese oxide (MnO_2) inevitably formed from an alternative reduction pathway of MnO_4^- (see eq. 4- 9). Solid MnO_2 could not be filtered out of the anaerobic cell since exposure to the air had an immediate reducing effect on the enzyme. Therefore, the light-scattering contribution of MnO_2 had to be calculated and subtracted from the absorbance spectra. The value obtained for the extinction coefficient of 100% oxidized wild type human Mn-SOD at 480nm was $\epsilon = 600 \pm 20\ M^{-1}cm^{-1}$.

Self-mediation of human Mn-SOD

The ability of human Mn-SOD to self-mediate with the redox electrode was measured to determine if mediators were needed (as it is the case in *E. coli* Mn- and Fe-

SODs). Human Mn-SOD was introduced in the anaerobic chamber at 1 mM concentration and degassed. The enzyme was then reduced in a stepwise fashion using dithionite as the reducing agent. Spectral and potentiometric data were recorded one to three hours after each addition of titrant. Figure 4-2 shows that, as the dithionite reduced the enzyme, the visible absorbance of Mn^{3+} (with a maximum at 485nm) decreased accordingly. However, the potential readings after optical equilibration were random and the plot of absorbance versus potential (inset of figure 4-2) could not be fit to the Nernst equation. Therefore human Mn-SOD under these conditions cannot self-mediate and the determination of its midpoint potential (E_m) requires the presence of a mediator.

Mediators

Titration of mediator alone was performed to check for solubility and stability in 100 mM phosphate buffer, extinction coefficients, and midpoint potential. As mentioned earlier in this Chapter, only ferricyanide and pentacyanoaminoferrate were suitable to measure the redox potential of human Mn-SOD. Table1 lists all the mediators tried in this study. Interestingly, cobalt-EDTA did not interact with the enzyme even though its solubility, size and potential was within range.

The extinction coefficients at optical signatures of $Fe(CN)_6$ and $Fe(CN)_5NH_3$ were measured in 100 mM KH_2PO_4/100mM KCl pH 7.8, and are reported in Table 4-2. Those values were in good agreement with reported values (Stankovich, personal communication; Burgess, 1988) even though the midpoint potential of a redox group varies greatly with temperature, buffer and salt concentration.

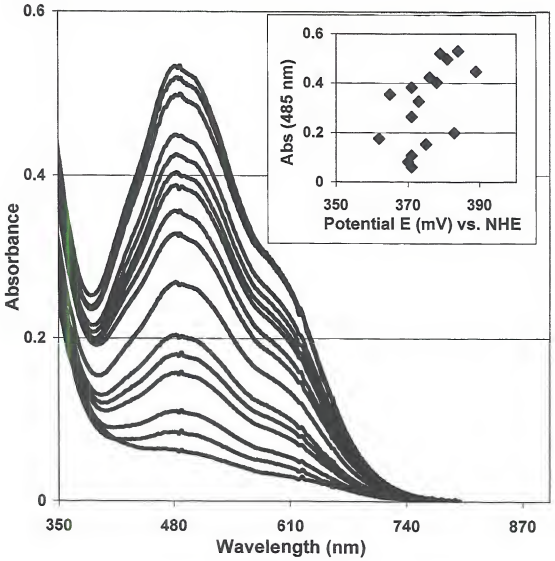


Figure 4-2: Reductive titration of human Mn-SOD by dithionite without a mediator. The enzyme is initially 90% oxidized (top trace) and is gradually reduced by stepwise addition of dithionite. Potential was recorded 1 to 8 hour(s) after each addition of dithionite. The plot of the absorbance versus potential (inset) does not follow a Nernstian behavior and the midpoint potential of human Mn-SOD could not be derived from this experiment. [human Mn-SOD]= 1 mM in 100mM KH_2PO_4/100mM KCl. The enzyme was degassed and kept under a nitrogen environment.

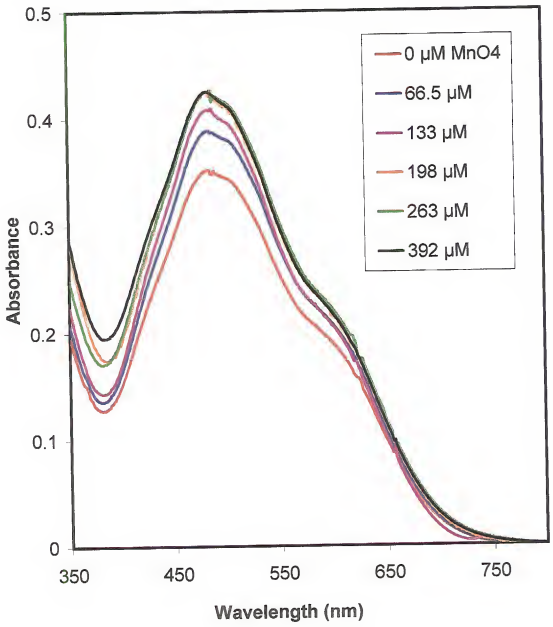


Figure 4-3: Oxidation of Mn-SOD with permanganate. Three milliliters of freshly purified human Mn-SOD (red) was treated with increasing amounts of MnO_4^- (see inset) until no more change in the oxidation state of the enzyme was visible. The sample was equilibrated for up to 1 hour after each addition of permanganate before collecting data. The enzyme concentration was corrected *a postiori* due to change in volume. $[Mn\text{-}SOD]_{initial}$ = 700 µM in 100 mM KH_2PO_4/100mM KCl pH 7.8.

Single point experiments

The two successful mediators – $Fe(CN)_6$ and $Fe(CN)_5NH_3$ – were used separately to calculate the intrinsic redox potential of human Mn-SOD by single point equilibrium experiments. Figure 4-4a shows a slow redox equilibration between fully oxidized $Fe(CN)_6$ and partially reduced enzyme. From the spectral data, we observed a reoxidation of Mn^{2+} enzyme to Mn^{3+} from the absorbance at 485nm, and a corresponding reduction of the mediator from the absorbance at 421nm (Figure 4-4b), which shows that the two mediators first act as titrants by pulling electrons away from the metal active site. This process is very slow partly because of the size of the mediator that is much bigger than superoxide. For that reason, the mediator may have limited access to the metal center. Equilibrium was reached after up to 35 hours depending on the reduction state of the enzyme when mixed with fully oxidized mediator. At equilibrium, the mediator served as an electron bridge between the enzyme and the electrode. The ambient potential and the ratio of concentrations of oxidized to reduced enzyme was substituted into the Nernst equation to derive the midpoint potential of human Mn-SOD, E_m. Four experiments were conducted using $Fe(CN)_6$ as a mediator (Figure 4-4a), and consistently gave a midpoint potential of 407mV (± 24 mV) for human Mn-SOD (Figure 4-4b).

Three similar experiments were conducted using $Fe(CN)_5NH_3$ as a mediator (Figure 4-5). In this case, the oxidation state of the mediator was followed at 397nm. The equilibration time between $Fe(CN)_5NH_3$ and the enzyme was longer than $Fe(CN)_6$ and the enzyme. Consequently, the amount of data retrievable using $Fe(CN)_5NH_3$ as a mediator was less due to enzyme degradation. Also, the amplitude of the change in absorbance of the enzyme was less compared to experiments using $Fe(CN)_6$ as a

Table 4-1: Potential mediators tested for the electrochemical titration of human Mn-SOD. Only $Fe(CN)_6$ and $Fe(CN)_5NH_3$ were appropriate mediators for human Mn-SOD.

Chemical name	Midpoint potential E_m (mV)	Signature peaks (nm)	Solublility in 100 mM KH_2PO_4 pH 7.8
$CuCl_2$	≅ 380	N.A.	≈ 300 μM
Cu-EDTA	<100	345	> 50 mM
Cu-DTPA	≅ 200	375	> 100 mM
Cu-Citrate	≅ 100	350	> 50 mM
$FeSO_4$	≅ 770	N.A.	≈ 200 μM
Fe-EDTA	120	445	> 50 mM
Fe-DTPA	≅ 300	495	> 100 mM
Fe-Citrate	???	360	> 100 mM
$CoCl_2$	≅ 1000	N.A.	< 700 μM
Co-EDTA	≅ 380	380, 520	> 100 mM
Co-DTPA	≅ 360	490	≈ 500 μM
Co-citrate	???	530	> 100 mM
DCIP	217	605	> 100 mM
$Fe(CN)_6$	435	421	> 500 mM
$Fe(CN)_5NH_3$	403	397	> 500mM

Table 4-2: Midpoint redox potentials (E_m) and extinction coefficients (ε, oxidized form) of mediators used in this study to measure the midpoint potential of human Mn-SOD. Each wavelength ("signature peak") represents a peak of absorbance characteristic of the mediator.

Mediator	Midpoint potential[(1)] E_m (mV)	Signature peak[(2)] (nm)	Ext. coeff.[(2)] ε ($M^{-1}cm^{-1}$)
$Fe(CN)_6$	435mV	421	971
		421	4.7 (reduced form)
$Fe(CN)_5NH_3$	403mV	397	1,200

(1) Values obtained by electrochemical titration.

(2) Values calculated under the following conditions: 100mM KH_2PO_4/100mM KCl, pH 7.8, 25 °C.

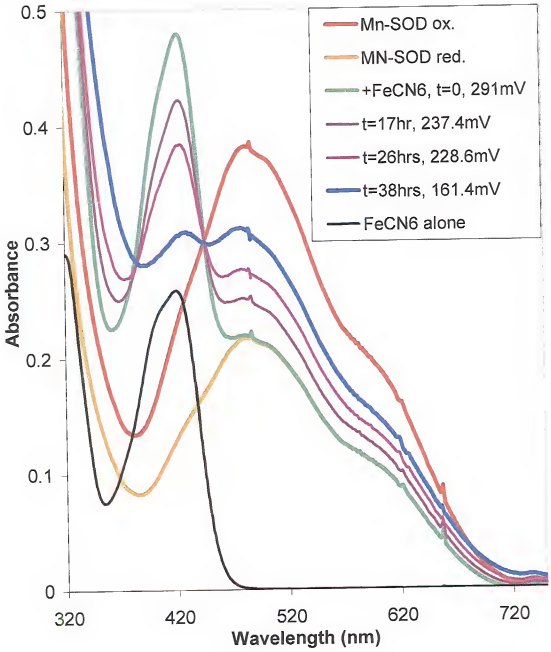


Figure 4-4a: Single point titration of human Mn-SOD with $Fe(CN)_6$. The absorbance of the enzyme and the mediator is ploted versus wavelength. [Mn-SOD] = 700 μM, $Fe(CN)_6$ = 250 μM. Enzyme (—) was partially reduced (—) with H_2O_2. Time zero is defined at the addition of $Fe(CN)_6$ (—) after which enzyme and mediator were allowed to interact up to 38 hours (—). $Fe(CN)_6$ alone (—) is shown as a reference.

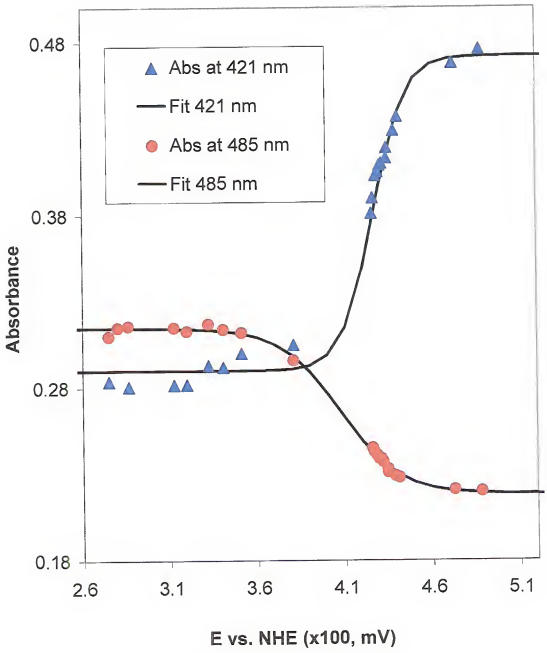


Figure 4-4b: Single-point titration of human Mn-SOD with $Fe(CN)_6$. The absorbance at signature peaks for human Mn-SOD (red, 485nm) and $Fe(CN)_6$ (blue, 421nm) is plotted versus potential. This data was derived from figure 4-4a. The midpoint potentials for $Fe(CN)_6$ and human Mn-SOD were calculated by fitting the data to the Nernst equation using the software Enzfitter® giving the following values: E_m ($Fe(CN)_6$) = 427 ± 13 mV; E_m (human Mn-SOD)= 407 ± 21 mV.

mediator. Because of this difference, a figure such as Figure 4-4b could not be made for $Fe(CN)_5NH_3$, and the midpoint potential of the enzyme was derived from the equilibrium trace (See figure 4-5). The midpoint potential E_m found for human Mn-SOD from two separate experiments using $Fe(CN)_5NH_3$ as a mediator was 372 mV and 383 mV. This result is on average 25 mV lower than by using $Fe(CN)_6$ and probably represents a lower limit for the midpoint potential of the enzyme. Nevertheless, these experiments demonstrate that both ferricyanide and pentacyanoaminoferrate can act as mediators with the active site metal of human Mn-SOD to determine the midpoint potential of the enzyme.

Redox titration

In order to check for the reversibility and Nernstian behavior of the intrinsic redox potential of human Mn-SOD obtained by single point equilibration, I conducted full redox titrations using dithionite and permanganate as reducing and oxidizing agents, respectively. The enzyme was equilibrated with ferricyanide (10:1, enzyme:mediator) and titrated by stepwise addition of titrant. The fraction of enzyme in the oxidized state was calculated from the spectral data and correlated to the measured ambient redox potential. Initially, the enzyme was 90% oxidized and gradually reduced until the potential dropped to 250 mV versus NHE (Figure 4-6a). The data was then fit to the Nernst equation and the midpoint potential was derived (figure 4-6b). Following this reductive titration, an attempt was made to reoxidize the enzyme by stepwise addition of permanganate. However, the reoxidation of human Mn-SOD was complicated by simultaneous enzyme degradation and formation of manganese oxide as mentioned earlier (see equation 4-9). Therefore, the amount of information retrievable during reoxidation of the sample with permanganate (Figure 4-7a) was less than during

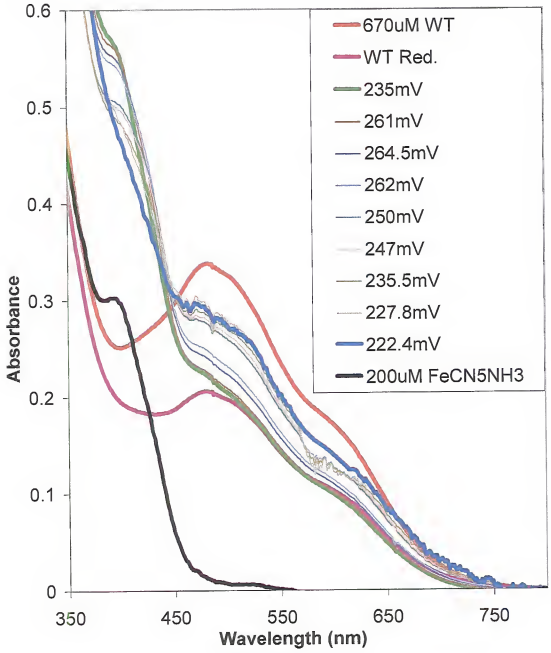


Figure 4-5: Single point titration of human Mn-SOD with $Fe(CN)_5NH_3$. The absorbance of the enzyme and the mediator is ploted versus wavelength. [Mn-SOD] = 670 μM, $Fe(CN)_5NH_3$ = 250 μM. Enzyme (—) was partially reduced with H_2O_2 (—). Time zero is defined at the addition of $Fe(CN)_5NH_3$ (—), after which enzyme and mediator were allowed to interact up to 45 hours (—). $Fe(CN)_5NH_3$ alone (—) is shown as a reference.

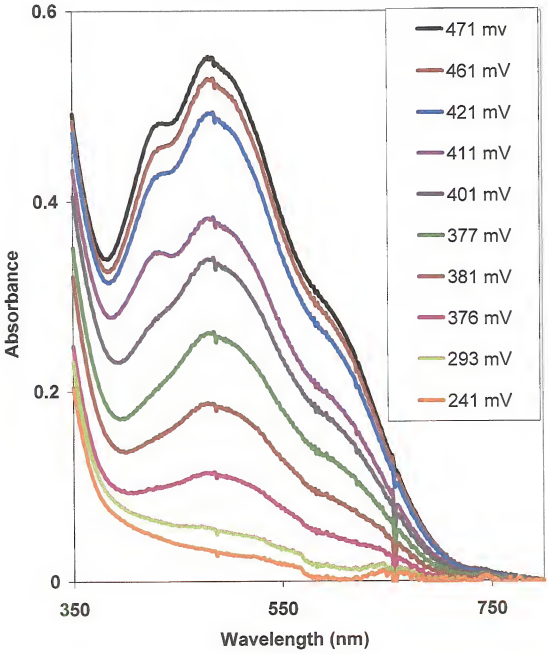


Figure 4-6a: Reductive titration of human Mn-SOD with dithionite using $Fe(CN)_6$ as a mediator. Oxidized human Mn-SOD at 1 mM concentration was mixed with 100 μM $Fe(CN)_6$ fully oxidized. The ambient potential was recorded 1 to 8 hours after each addition of dithionite (see inset). A limited number of traces are shown for clarity.

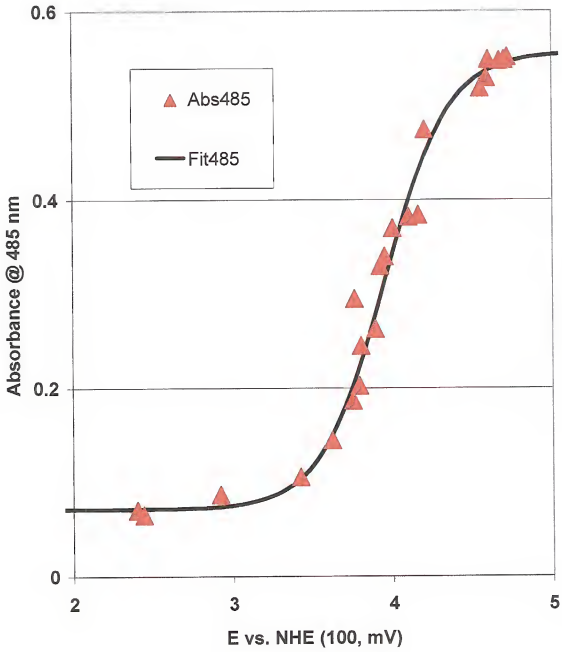


Figure 4-6b: Absorbance of human Mn-SOD at 485 nm versus potential. These data are derived from Figure 4-6a and were fitted to the Nernst equation by using the software Enzfitter® assuming one electron transfer between the enzyme and the mediator. Absorbance at 485 nm was not complicated by the change in absorbance of the $Fe(CN)_6$ at 421nm since this mediator has no residual absorbance at 485nm. From this fit, E_m for human Mn-SOD was determined to be 395 ± 19 mV.

reduction by dithionite, and could not be fit to the Nernst equation (Figure 4-7b). The activity of the enzyme was determined periodically using stopped-flow spectroscopy. On average, 30 to 50% of the enzyme was degraded during the redox titration, based on the absorption of the enzyme at 280 nm.

The E_m for human Mn-SOD obtained by the reductive titration and iterative fits to the Nernst equation was 395 ± 19 mV, which is in good agreement with the E_m calculated from single point equilibrium experiments (407 ± 21 mV). Unfortunately, I was unable to efficiently reoxidize the enzyme with permanganate. Therefore, the reversibility of the Nernstian behavior could not be checked.

Discussion

The midpoint redox potential (E_m) of human Mn-SOD was found by electrochemical titration to be E_m = 393 ± 35 mV (when combining all the data from the two different mediators). This potential is almost exactly half way between the midpoint potential of the oxidation of superoxide to oxygen (-160 mV, eq. 4-3) and that of the reduction of superoxide to hydrogen peroxide (+850 mV, eq. 4-5). It is also higher than that of *E. coli* Mn-SOD by roughly 100mV (Vance, 1999). The central position of the redox potential of human Mn-SOD compared to the reductive and oxidative reactions of superoxide suitably places the enzyme for the catalysis of both reactions by making each one of them thermodynamically favorable. Since the potential of free manganese in solution is +1500 mV, an essential role of the enzyme is to reduce the midpoint potential by 1100 mV down to 400 mV through coordination with the ligands and the active site environment. Without this adjustment, the reduction of superoxide to hydrogen peroxide would not be

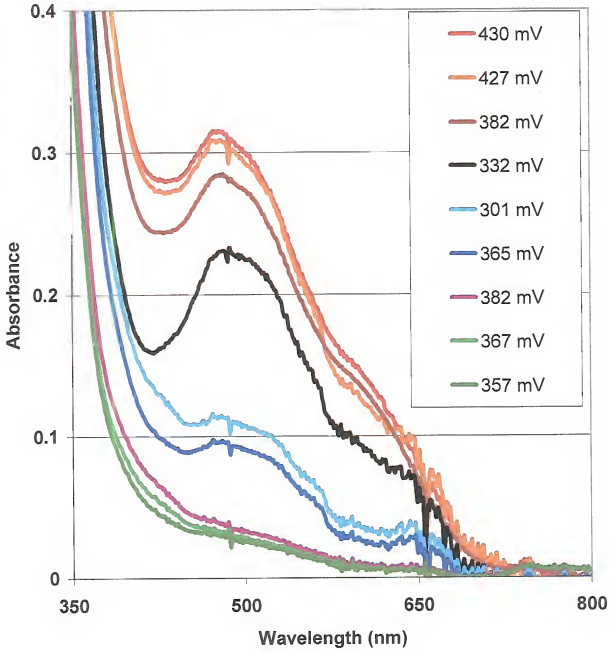


Figure 4-7a: Oxidative titration of human Mn-SOD with permanganate using $Fe(CN)_6$ as a mediator. Reduced human Mn-SOD (═) at 1 mM was initially mixed in a 10 fold excess with 100 μM $Fe(CN)_6$ in the reduced form. The potential was recorded 1 to 8 hours after each addition of permanganate until the potential reach 430 mV (═). The enzyme concentration was checked during the experiment and corrected to account for enzyme degradation. These data could not be fitted to the Nernst equation because of enzyme degradation.

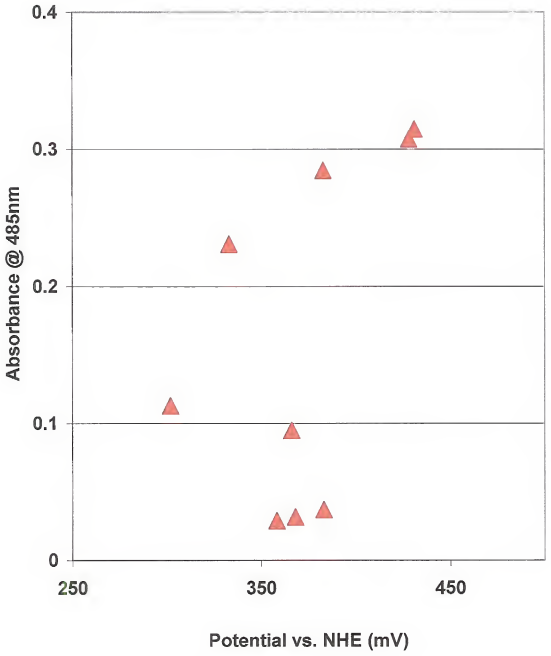


Figure 4-7b: Absorbance at 485 nm of human Mn-SOD versus ambient potential. These data are derived from figure 4-7a and could not be fit to the Nernst equation due to enzyme degradation.

thermodynamically favorable since the potential of the oxidation of Mn^{2+} to Mn^{3+} would be higher than that of the reduction of superoxide to hydrogen peroxide.

When freshly isolated from its overexpression in *E. coli* cells, human Mn-SOD is mostly oxidized (90 ± 5%). However, after a few days, the enzyme becomes partially reduced and stabilizes around an oxidation state of about 80% in storage buffer under atmospheric pressure. As a consequence, determining the extinction coefficient of Mn^{3+}-SOD (at its peak of 480nm in the visible range) has been a challenge. Many investigators have attempted to explain why Mn-SOD becomes partially reduced in an apparent oxidative environment, and how the enzyme can be reoxidized (Lawrence and Sawyer, 1979; St.Claire et al., 1991). Unlike Fe-SOD, which is readily oxidized in the presence of pure oxygen gas, Mn-SOD is rather unaffected and may only be partially reoxidized in a period of many days by this method. This side effect did not prevent us from accurately measuring the extinction coefficient of the enzyme. We found that, for 100% oxidized human Mn-SOD, $\varepsilon_{480} = 600\ M^{-1}cm^{-1}$. This value is higher than that previously reported (Hsu et al., 1995), and the difference might be due to errors in the estimation of the oxidize state of the enzyme.

The ability of human Mn-SOD to equilibrate with the redox electrode in the absence of mediators was ruled out. Reductive titration of the enzyme by dithionite showed that, as the enzyme went from fully oxidized to 85% reduced, the potential readings did not follow a Nernstian behavior but stayed fairly stable by ranging randomly from 360 to 390mV. This demonstrated the lack of communication between the redox electrode and the active site metal, and the need for an electron bridge. Two mediators, ferrycianide $Fe(CN)_6$ and pentacyanoaminoferrate $Fe(CN)_5NH_3$, were found to be

suitable for measuring the redox potential of human Mn-SOD. For each mediator, the redox potential of the enzyme was measured through single equilibrium experiments in which fully oxidized mediator was mixed with partially reduced enzyme and allowed to equilibrate. The equilibration time was very slow, which can be explained by the size of the mediators compare to superoxide. Since both $Fe(CN)_6$ and $Fe(CN)_5NH_3$ are much bigger than superoxide, their size may limit their accessibility to the metal buried in the active site. In addition, Vance (1999) reported that $Fe(CN)_6$ is not suitable as a mediator for *E.coli* Mn-SOD, which can be explained by the 150 mV difference between their respective midpoint potentials. The successful mediation of $Fe(CN)_6$ with human Mn-SOD was at first unexpected. Indeed, we did not anticipate that the midpoint potential of the human enzyme would be 112 mV higher than that of its bacterial homologue, which brings human Mn-SOD within the range of $Fe(CN)_6$ (since the midpoint potential of this mediator is 435 mV). Therefore, even though it is not clear why the two enzymes have different midpoint potentials, the requirement for different mediators can be explained by the significant difference in their midpoint potentials.

The midpoint potential of human Mn-SOD was also measured through a full redox titration in order to satisfy the requirements of the Nernstian behavior. In these experiments, ferricyanide was chosen as a mediator for its superior stability and spectral signatures over pentacyanoaminoferrate. Dithionite was used as the reducing agent. It is a commonly used titrant because of its lack of absorbance in the visible range and strong reducing power (E_m = -750mV). Permanganate ($KMnO_4$) was used as the oxidative agent despite its tendency to break down to manganese oxide over time, limiting the amount of collectable data. The oxidative titration of human Mn-SOD with MnO_4^- was inconclusive

because of enzyme degradation and the formation of manganese oxide. However, the reductive titration was in close agreement with the single point equilibrium experiments. Table 4-3 summarizes the values for the redox potential of human Mn-SOD obtained by the two different methods.

The redox potential measurements of human Mn-SOD were very difficult and one more example of the notorious challenge involved in electrochemical measurements with non-electron carrier proteins. Nevertheless, two different approaches using two different mediators gave consistent results. Three of the four main criteria for determining a reduction potential were fulfilled: (1) The same E_m was obtained using two distinct mediators, each with different spectral and redox characteristics; (2) the same E_m was obtained from single point titrations and reductive titrations; and (3) the reductive titration followed Nernstian behavior. Reversibility of the Nernstian behavior could not be verified. In the future, the redox potential of the wild type enzyme could be used as a reference when measuring the redox potential of site-specific mutants. For instance, it would be very interesting to compare the midpoint potential of wild-type Mn-SOD with that of Q143 mutants for which the redox state of the metal in the resting state is obviously greatly altered (Lévêque *et* al., 2000). Therefore, this work on the wild-type enzyme opens a new area of research where the goal will be to delineate the role of Q143 and other active site residues in the fine tuning of the redox potential in the wild type enzyme.

Table 4-3: Intrinsic redox potentials obtained in this study through single point (S.P.) and reductive titrations.

	E_m alone (mV)	E_m S.P. titration (mV)	E_m reductive titration (mV)
$Fe(CN)_6$	435 ± 13 mV	427 ± 13 mV	N/A
$Fe(CN)_5NH_3$	403 ± 12 mV	398 ± 18 mV	N/A
Mn-SOD	N/A	407 ± 21 mV[(1)] 377 ± 6 mV[(2)]	395 ± 19 mV

(1) Using $Fe(CN)_6$

(2) Using $Fe(CN)_5NH_3$

CHAPTER 5
CONCLUDING REMARKS AND FUTURE DIRECTIONS

In this dissertation, I have addressed the function in catalysis of two active-site residues in human Mn-SOD. This work provides the first discussion of the effect on catalysis and on the physical properties of Mn-SOD caused by the replacement of Gln143 and His30 with many residues. My studies characterize the catalysis of these mutants using a wide variety of approaches (X-ray crystallography, redox potential measurements, scanning calorimetry, pulse radiolysis, and stopped-flow spectrophotometry) performed in our laboratory and through collaborations. Using these techniques, this study adds to the accumulated knowledge of Mn-SOD by providing new insights into the active-site topology. For example, the crystal structure of the mutant Gln143Ala showed two water molecules occupying the sites of the OЄ and NЄ of the glutamine of the wild type. Although these substituted water molecules maintain the overall hydrogen-bonded network in the active site, both the catalytic activity and the redox state of the Gln143Ala mutant were very significantly affected (*Chapter 2*, and Figure 5-1). This indicates that part of the role of the active site residues is to sequester the metal from bulk solvent molecules. It may account for the sterically constrained nature of the active site that effectively excludes water. It also shows that proton transport to the active site is not efficient through a hydrogen-bonded water chain, contrary to the case of carbonic anhydrase (Lindskog, 1997) or the gramicidin channel (Pomes and

Roux, 1996). In addition, buffer rescue experiments (where small exogenous proton donors are used in an attempt to restore proton transfer) failed to show an increase in activity for any of the Gln143 mutants tested (data not shown). Therefore, the decrease in activity might not be due to an alteration in the proton transfer *per se*, but to an alteration of the redox state of the enzyme. This alteration would then decrease the activity by affecting the ability of the enzyme to participate in the oxidation-reduction cycles necessary for catalysis.

In contrast to the data on Q143A in which the hydrogen-bonded network was maintained by intervening water molecules, the mutant H30N interrupts the hydrogen-bonding network but maintains the topology in the first and second shell of the manganese. As shown in *Chapter 3*, the hydrogen-bonded array involving His30 that may be involved in the formation of hydrogen peroxide in the wild-type enzyme is interrupted by the mutation H30N, possibly forcing the proton transport to follow an alternative pathway. Consequently, the value of k_{cat} and k_{cat}/K_m for the H30N mutant was decreased about 10 fold compared to wild type during the first few milliseconds of the reaction. However, the catalytic rate of the H30N mutant was shown to be faster than that of the wild type enzyme in the entire progress curve of catalysis because the wild type enzyme becomes product inhibited and enters a zero order phase while the mutant enzyme remains first order (under nonsaturating conditions). Therefore, H30N is most likely a more efficient enzyme than the wild type because of the build up of the product-inhibited complex in wild type enzyme (Figure 5-1). Mutations at both residues, 143 and 30, have profound effects on product inhibition of Mn-SOD and demonstrate the dependence of this inhibition on surrounding residues.

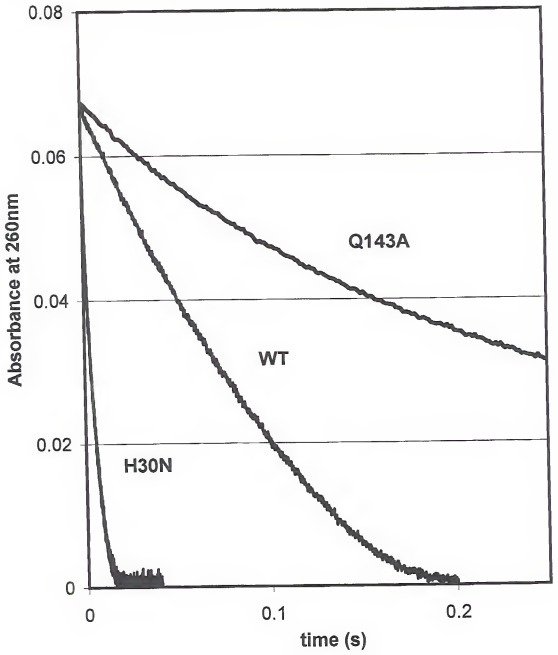


Figure 5-1: Overlay spectra of pulse radiolysis traces of wild type (WT), Gln143Ala (Q143A), and His30Asn (H30N) human Mn-SOD. The absorbance of superoxide at 260 nm is plotted versus time. Each enzyme is at 1 μM concentration. Conditions were 2 mM TAPS pH 8.2, 30 mM formate, 50 μM EDTA. Each trace was corrected for metal content.

One may wonder why nature selected a product-inhibited enzyme for human mitochondria over a non-inhibited one such as Fe-SOD. An answer might be found in the requirement for synchronized enzymatic activity. In high eukaryotes, Mn-SOD activity is in balance with the activity of catalase and peroxidase, which further detoxifies the cell by converting the hydrogen peroxide produced by Mn-SOD to oxygen and water. Elevated levels of SOD activity are detrimental to the cell when not in balance with catalase and peroxidase, and have been linked to Down's syndrome (Summitt, 1981). It would therefore be interesting to determine whether expression of H30N Mn-SOD would provide better cytoprotection than wild type in human cells. We can anticipate that a similar misbalance may arise if the production of hydrogen peroxide by the H30N mutant is significantly greater than that by wild type. We might even speculate that in wild-type Mn-SOD, the formation of the product-inhibited complex prevents over production of hydrogen peroxide by slowing down the catalytic rate of the enzyme at high substrate concentrations. In addition, the activity of wild type human Mn-SOD is maximal for the first few milliseconds of the reaction, which is in the same time scale as the existence of superoxide under physiological conditions. Therefore, genetic transfection of H30N Mn-SOD in human cells may require co-transfection of the gene coding for catalase and/or peroxidase to insure a complete removal of all forms of oxygen free radicals.

The clinical potential of H30N Mn-SOD in gene therapy research is currently being evaluated in collaboration with Chris Davis (Biochemistry Department, UF) and Dr. Agarwal (Department of Medicine, UF). As mentioned earlier, Figure 5-1 clearly demonstrates the first order kinetics of H30N and Q143A as well as the increased efficiency of the H30N mutant over the wild type enzyme. To further address the

effectiveness of both H30N and Q143A, we have generated mammalian expression vectors containing the WT, Q143A, and H30N human Mn-SOD cDNAs. We then evaluated the physiological efficiency of these proteins following transient transfection in a TNF cytotoxic assay. Preliminary data of cell survival using HEK 293 cells were obtained following transfection with either vector alone or overexpression of the WT, the Q143A, or the H30N construct. From these data, cells expressing the H30N mutant show approximately 10 to 15 % increase survival compared to WT human Mn-SOD. This result is very promising and more experiments are in progress.

In the long term, mutant enzymes that will have demonstrated successful cytoprotection improvement in cell cultures over the wild type enzyme could be used for gene therapy in animal models of inflammation. Gene transfer research has already shown some degree of success in phase III clinical results for genes involved in advanced metastatic melanoma (Stopeck, 1997), SCID-XI (an X chromosome-linked member of the SCID disorder involved in lymphocyte differentiation, Cavazzana-Clavo, 2000), and treatment of hemophilia (Kay, 2000). We might hope that gene therapy will be extended to a vast number of genes including that of Mn-SOD (for a list of SOD related pathologies, see introduction chapter).

This study, as well as other work in our laboratory (Guan et al., 1998) has provided valuable information on potential proton donors during catalysis. However, it is still unknown whether those residues work in concert or separately to deliver the hydrogens to the metal center. The study of double mutants, where the hydrogen bonding network is disrupted at two different locations might enhance our understanding of the active site synergy. If two potential proton donors work in concert during catalysis,

breaking the network at any single site should have the same effect as breaking it at both sites. Conversely, a second site mutation would decrease catalysis even further if the two residues contribute to two different proton transfer pathways. I have prepared two such mutants (H30N-Y34F and Q143E-Y34H) and obtained preliminary kinetic data in collaboration with Bill Greenleaf in our laboratory. The data shows that the double mutant H30N-Y34F is a slower enzyme than each of the two single mutants, indicating that those two residues might work separately in providing protons to the active site. The mutant Q143E-Y34H is still under investigation and more experiments are being planned including pH titrations and buffer rescue experiments.

In this work, I have focused on specific residues that were carefully chosen based on previous work and on their location in the active site, and I have generated mutations that were designed with a specific goal in mind. One very different approach to study Mn-SOD would be through gene shuffling (Stemmer, 1994). In this technique, a small group of closely related genes coding for the same enzyme (for example, human, cow, rat and *T. thermophilus* Mn-SODs), are cut with restriction enzymes, mixed, reassembled randomly through PCR, and cloned. The chimeric clones are expressed in bacteria and screened for activity. The best clones are then expressed in large scale and sequenced. By mixing genes that have branched out at different points through evolution, one can hope to generate chimera with equivalent or even better activity than any of the wild type enzymes. This powerful technique combines in one chimera the selective advantages acquired through evolution by different organisms. Besides the potential of creating higher-than-normal catalytic activity, this approach may also reveal important residues that have been conserved through evolution.

This study has demonstrated an important distinction between the midpoint potential of free manganese ion (E_m = + 1500 mV) and that of manganese bound in human Mn-SOD (E_m = + 400 mV). This 1100 mV difference is essential for the difference in potential (ΔE_m) between the enzyme and the reduction of $O_2^{\cdot -}$ to H_2O_2 (E_m = + 890 mV) to be positive (i.e. thermodynamically favorable). The fine tuning of this redox potential is very sensitive to the environment of the metal as shown by single mutations of the second shell residues in the active site (*Chapter 2*) and demonstrates that the five inner shell ligands are not the only players in the fine tuning of the redox potential of the enzyme. The very delicate design of the native enzyme and the adjustment of the electronic structure at the metal ion emphasize the role of the protein in optimizing electron transfer. As a future direction, it would be very interesting to measure the redox potential of the most active mutants at position 143 (Q143A and Q143N) and to compare their midpoint potentials with that of the wild type enzyme. An attempt could then be made to construct a free energy plot of the rate constant for catalysis versus the midpoint potentials (E_m) for several mutants of Mn-SOD. The rate constant used would have to be one limited by electron transfer (k_{cat}/K_m) as opposed to proton transfer (k_{cat}, since catalysis of wild-type Mn-SOD is partly diffusion controlled). There have been very many studies attempting to link a thermodynamic constant E_m with a kinetic constant such as k_{cat}/K_m, including Marcus theory (Marcus, 1968). This theory can be applied to proton transfer as well, in which case k_{cat} would be correlated with ΔpKa for donor and acceptors (Kresge, 1975). The present study has established the basis for the application of the Marcus theory to the electron and proton transfer during catalysis of human Mn-SOD.

Another interesting question is whether electron or proton transfer is rate limiting during catalysis by human Mn-SOD. Proton coupled electron transfer (known as PCET) has been the center of numerous investigations for the last few decades. From non-biological systems including the hydrogen ion discharge on a metal surface (H_3O^+ + e-(Metal) → $H_{aq.}$ +H_20; Levich, 1970) to the in-depth study of metalloproteins (including the well described cytochrome c oxidase, Kitagawa and Ozura, 1997), many researchers have studied whether proton transfer is coupled to electron transfer. In the case of superoxide dismutases, a few active site residues (H30, Y34) are believed to participate in proton delivery, but the exact proton transfer pathways are still unknown. For electron transfer, the half reaction involving the reduction of Mn^{3+}-SOD to Mn^{2+} and the oxidation of superoxide to oxygen is believed to be a pure oxido-reduction reaction uncoupled to proton transfer (Scherk et al., 1996; Tierney et al., 1995). However, the reoxidation of Mn^{2+}-SOD to Mn^{3+} via reduction of superoxide to hydrogen peroxide is a more complex process involving PCET. Whether electron transfer drives the protonation of superoxide or *vice versa* is still unclear. Hopefully, comparing the effects of site directed mutant enzymes on both the redox potential and the kinetics of Mn-SOD will provide more information leading to understanding the intimate relationship between proton and electron transfer during catalysis.

REFERENCES

Asada, K., Kanematsu, S. and Uchida, K. (1977) *Arch. Biochem. Biophys.* **179,** 243.

Azab, H.A., Banci, L., Borsari, M., Luchinat, C., Sola, M. and Viezzoli, M.S. (1992) *Inorganic Chemistry* **31**, 4649.

Bannister, J.V., Bannister, W.H., and Rotilio, G. (1987) *CRC Crit. Rev. Biochem.* **22**, 111.

Barman, B.G. and Tollin, G. (1972) *Biochemistry* **25**, 4755.

Barrette, W.C., Jr., Sawyer, D.T., Fee, J.A. and Asada, K. (1983) *Biochemistry* **22**, 624.

Beck, Y., Bratfeld, D., Yavin, Z., Levanon, A., Gorecki,M., and Hartman, J.R. (1988) *Biotech.* **6**, 930.

Beem, K. M., Richardson, J.S., and Richardson, D.C. (1976) *J. Mol. Biol.* **105**, 327.

Benov, L. and Fridovich, I. (1995) *J. Bacteriol.* **177**, 3344.

Beyer, W., Imlay, J. and Fridovich, I. (1991) *Prog. Nucleic Acid Res. Mol. Biol.* **40**, 221.

Borders, C.L. Jr., Bjerrum, M.J., Schirmer, M.A., and Oliver, S.G. (1998) *Biochemistry* **37,** 11323.

Borgstahl, G.E.O., Parge, H.E., Hickey, M.J., Beyer, W.F., Hallewell, R.A., and Tainer, J.A. (1992) *Cell* **71**, 107.

Borgstahl, G.E., Parge, H.E., Hickey, M.J., Johnson, M.J., Boissinot, M., Hallewell, R.A., Lepock, J.R., Cabelli, D.E. and Tainer, J.A. (1996) *Biochemistry* **35**, 4287.

Bostantjopoulou, S., Kyriazis, G., Katsarou, Z., Kiosseoglou, G., Kazis, A., and Mentenopoulos, G. (1997) *Funct. Neurol.* **12,** 63.

Bridges, S.M. and Salin, M.L. (1981) *Plan Physiol.* **68**, 275.

Bruch, R.C. and Thayer, W.S. (1983) *Biochim Biophys Acta* **733**, 216.

Bull, C. and Fee, J.A. (1985) *J. Am. Chem. Soc.*, **107**, 3295.

Bull, C., Niederhoffer, E.C., Yoshida, T., and Fee, J.A. (1991) *J. Am. Chem. Soc.* **113**, 4069.
Burgess, J. (1988) Ions in Solution, Ellis Horwood Limited, Chichester, England.

Cabelli, D.E., Guan, Y, Leveque, V., Hearn, A.S., Tainer, J.A., Nick, H.S. and Silverman, D.N. (1999) *Biochemistry* **38**, 11686.

Cavazzana-Clavo, M. (2000) *Science* **288**, 669.

Cerutti, P.A. (1985) *Science* **227**, 373.

Cerutti, P.A. and Trump, B.F. (1991) *Cancer Cells* **3**, 1.

Chance, B., Sies, H. and Boveris, A. (1979) *Physiol. Rev.* **59**. 527.

Crapo, J.D. and Tierney, D.F. (1974) *Amer. J. Physiol.* **226**, 1401.

Deng, H.X., Tainer, J.A., Mitsumoto, H., Ohnishi, A., He, X., Hung, W.Y., Zhao, Y., Juneja, T., Hentati, A., and Siddique, T. (1995) *Hum. Mol. Genet.* **4**, 1113.

DiGuiseppi, J. and Fridovich, I. (1984) *Crit. Rev. Toxicol* **12**, 315.

Duke, M.V. and Salin, M.L. (1985) *Arch. Biochem. Biophys* **243**, 305.

Dutton, P.L. (1978) *Methods Enzymol.* **54**, 411.

Estévez, A.G., Crow, J.P., Sampson, J.B., Reiter, C., Zhuang, Y., Richardson, G.J., Tarpey, M.M., Barbeito, L., and Beckman, J.S. (1999) *Science* **286**, 2498.

Farr, S. B., D'Ari R. and Touati, D. (1986) *Proc. Natl. Acad. Sci. USA* **83**, 8268.

Frank, L. and Massaro, D. (1980) *Am. J. Med.* **69**, 117.

Fielden, E.M., Roberts, P.B., Bray, R.C., Lowe, D.J., Mautner, G.N., Rotilio, G., and Calabrese, L. (1974) *Biochem. J.* **139**, 49.

Fridovich, I. (1978) *Science* **201**, 875.

Fridovich, I. (1981) *Prog. Clin. Biol. Res.* **51**, 153.

Fridovich, I. (1985) The Harvey lectures, Series **79**, Academic Press, N.Y., 51.

Gregory, E.M. and Fridovich, I. (1973) *Bacteriol.* **114**, 543.

Gregory, E.M. (1985) *Arch. Biochem. Biophys.* **220**, 293.

Guan, Y., Hickey, M.J., Borgstahl, G.E.O., Hallewell, R.A., Lepock, J.R., O'Connor, D., Hsieh, Y, Nick, H.S., Silverman, D.N. and Tainer, J.A. (1998) Biochemistry **37**, 4722.

Gutteridge, J.M. and Halliwell, B. (1990a) *Trends Biochem. Sci.* **15**, 129.

Gutteridge, J.M. and Halliwell, B. (1990b) *Arch. Biochem. Biophys.* **283**, 223.

Halliwell, B. and Gutteridge, J.M. (1990) *Methods Enzymol.* **186**, 1.

Hawkridge, F.M. and Kuwana, T. (1973) *Anal Chem.* **46**, 1021.

Hearn, A.S., Tu, C.K., Nick, H.S., and Silverman, D.N. (1999) *J. Bio. Chem.* **274**, 24457.

Hendler, R.W. and Shrager, R.I. (1979) *J. Biol. Chem.* **254**, 11288.

Homma, Y., Tsunoda, M. and Kasai, H. (1994) *Bioch. Biophy. Res. Com.* **203**, 1063.

Hsieh, Y., Guan, Y., Tu, C.K., Bratt, P.J., Angerhofer, A., Lepock, J.R., Hickey, M.J., Tainer, J.A., Nick, H.S. and Silverman, D.N. (1998) *Biochemistry* **37**, 4731.

Hsu, J.-L., Hsieh, Y., Yu, C., O'Connor, D., Nick, H.S. and Silverman, D.N. (1996) *J. Bio. Chem.* **271**, 17687.

Hunter, T., Ikebukuro, K., Bannister, W.H., Bannister, J.V., and Hunter, G.J. (1997) *Biochemistry* **36**, 4925.

Imlay, J.A. and Fridovich, I. (1992) *J Bacteriol* **174**, 953.

Jackson, S.M.J. and Cooper, J.B. (1998) *Biometals* **11**, 159.

Kalyanaraman, B., Mason, R.P., Tainer, B., and Eling, T.E. (1982) *J. Bio. Chem.* **257**, 4764.

Kaprzak, K.S. (1991) *Chem. Res. Tox.* **4**, 604.

Kay, M.A. (2000) *Nature Genetics* **24**, 257.

Kim, F.J.; Kim, H.P.; Hah, Y.C. and Roe, J.H. (1996) *Eur. J. Biochem.* **241**, 178.

Kitagawa, T. and Ozura, T. (1997) *Prog. Inor. Chem.* **45**, 431.

Kresge, A.J. (1975) *Accounts of Chem. Res.* **8**, 354.

Kwiatowski, J.K., Safianowski, A., Kaniuga, Z. (1985) *Eur. J. Biochem.* **146**, 459.

Lah, M.S., Dixon, M.M., Pattridge, K.A., Stallings, W.C., Fee, J.A. and Ludwig, M. L. (1995) *Biochemistry* **34**, 1646.

Lawrence, G.D. and Sawyer, D.T. (1979) *Biochemistry* **18**, 3045.

Leatherbarrow, R.J. (1987) *Enzfitter*, Elsevier BIOSOFT, Cambridge, United Kingdom.

Lévêque, V. J.-P., Stroupe, M.E., Lepock, J.R., Cabelli, D.E., Tainer, J.A., Nick, H.S., and Silverman, D.N. (2000) *Biochemistry* **39**, 7131.

Lever, A.B.P. and Gray, H. B. (1978) *Amer. Chem. Soc.* **11**, 348.

Levich, V.G. (1970) *Physical Chemistry - An Advance Treatise*, ed. H. Henderson, W. Yost, **9B**, 985-1074, New-York: Academic.

Li, Y., Huang, T.T., Carlson, E.J., Melov, S., Ursell, P.C., Olson, J.L., Noble, L.J., Yoshimura, M.P., Berger, C., Chan, P.H., Wallace, D.C., and Epstein, C.J. (1995) *Nature Genetics* **11**, 376.

Lindskog, S. (1997) *Pharmacol. Ther.* **74**, 1.

Marcus, R.A. (1968) *J. Phys. Chem.* **72**, 891.

Marklund, S. (1976) *J. Biol. Chem.* **251**, 7504.

Martin, M.E., Byers, B.R., Olson, M.O.J., Salin, M.L., Archeneaux, J.E.L., and Tolbert, C. (1986) *J. Bio.Chem.* **261**, 9361.

McAdam, M.E., Fox, R.A., Lavelle, F., and Fielden, E.M. (1977a) *Biochem. J.* **165,** 71.

McAdam, M.E., Levelle, F., Fox, R.A., and Fielden, E.M. (1977b) *Biochem. J.* **165,** 81.

McClune, G.J. and Fee, J.A. (1976) *FEBS Lett* **67**, 294.

McClune, G.J. and Fee, J.A. (1978) *Biophys. J.* **24**, 65.

McRee, D.E. (1992) *J. Mol. Graph.* **10**, 44.

McRee, D.E. (1999) *J. Struct. Biol.* **125**, 156.

Mechler, F., Imre, S., and Dioszeghy, P. (1984) *J. Neurol. Sci.* **63,** 279.

Meier, B., Barra, D., Bossa, F., Calabrese, L., and Rotilio, G. (1982) *J. Bio Chem.* **257**, 13977.

Navaza, A. (1994) *Acta Crystallogr. A.* **50**, 157.

Otwinowski, Z. and Minor, W. (1997) *Methods Enzymol.* **276**, 307.

Padmanabhan, R.V., Gudapaty, R., Liener, I.E., Schwartz, B.A., and Hoidal, J.R. (1985) *Am. Rev. Respir. Dis.* **132**, 164.

Palma, J.M., Sandalio, L.M., and Del Rio, L.A. (1986) *J. Plant Physiol.* **125**, 427.

Pomes, R. and Roux, B. (1996) *Biophysical Journal* **21**, 19.

Puget, K. and Michelson, A.M., (1974) *Biochem. Biophys. Res. Commun.* **58**, 830.

Rabanini, J. and Nielson, S.O. (1969) *J. Phys.Chem.* **73**, 3736.

Ramilo, C.A., Leveque, V., Guan, Y., Lipock, J.R., Tainer, J.A., Nick, H.S. and Silverman, D.N. (1999) *J. Bio. Chem.* **274**, 27711.

Ringe, D., Petsko, G.A., Yamakura, F., Suzuki, K., and Ohmori, D. (1983) *PNAS* **80**, 3879.

Rosen, G.M., Pou, S., Ramos, C.L., Cohen, M.S., and Britigan, B.E. (1995) *FASEB J.* **9**, 200.

Salin, M.L. and Bridges, S.M. (1982) *Plant Physiol.* **69**, 161.

Sawyer, D.T., Sobkowiak, A. and Roberts, J.L., Jr. (1995) Electrochemistry for Chemists, John Wiley & Sons, Inc., New York, NY.

Scherk, C., Schmidt, M., Nolting, H.-F., Meier, B. and Parak, F. (1996) *European Biophysics Journal* **24**, 243.

Schnepf, E., and Brown, R.M., Jr. (1972) *Origin and Continuity of Cell Organelles*, (Reinert, J., and Ursprung, H., eds.), Spring-Verlag, New York.

Schwarz, H.A. (1981) *J. Chem. Educ.* **58**, 101.

Smith, M.W. and Doolittle, R.F. (1992) *J. Mol. Evol.* **34**, 175.

Sorkin, D.L. and Miller, A.-F. (1997) *Biochemistry* **36,** 4916.

St.Clair, C.S., Gray, H.B. and Valentine, J.S. (1991) *Inorganic Chemistry* **31**, 925.

Stadtman, E.R. (1991) *Am. J. Clin. Nutr.* **54**, 1125.

Stallings, W.C., Powers, T.B., Pattridge, K.A., Fee, J.A., and Ludwig, M.L. (1983) *PNAS* **80**, 3884.

Stallings, W.C., Pattridge, K.A., Strong, R.K., and Ludwig, M.L. (1985) *J. Biol. Chem.* **260**, 16424.

Stankovich, M.T. (1980) *Analytical Biochemistry* **109**, 295.

Steinman, H.M. (1982) *J. Bio. Chem.* **257**, 10283.

Steinman, H.M. (1985) *J. Bacteriol.* **162**, 1255.

Stemmer, W.P., (1994) *Nature* **370**, 389.

Stopeck, A.T. (1997) *J. Clinic. Onc.* **15**, 341.

Sturtevant, J.M. (1987) *Annu. Rev. Phys.Chem.* **38**, 463.

Summitt, R.L. (1981) Trisomy 21 (Down Syndrome): Research Perspectives, University Park Press.

Swartz, D.B. and Wilson, G.S. (1971) *Anal. Biochem.* **40**, 392.

Tainer, J.A., Getzoff, E.D., Richardson, J.S., and Richardson, D.C. (1983) *Nature* **306**, 284.

Thompson, J.A. and Hess, M.L. (1986) *Prog. Cardiovasc. Dis.* **28**, 449.

Tierney, D.L., Fee, J.A., Ludwig, M.L. and Penner-Hahn, J.E. (1995) *Biochemistry* **34**, 1661.

Valentine, J.S. and Curtis, A.B. (1975) *J. Am. Chem. Soc.* **97**, 224.

Vance, C.K. and Miller, A.-F. (1998a) *Biochemistry* **37,** 5518.

Vance, C.K. and Miller, A.-F. (1998b) *J. Am. Chem. Soc.* **120**, 461.

Vance, C.K. (1999) Thesis dissertation, Johns Hopkins University, Baltimore, Maryland.

Verhagen, M.F.J.M., Meussen, E.T.M. and Hagen, W.R. (1995) *Biochimica et Biophysica Acta* **1244**, 99.

Visner, G.A., Chesrown, S.E., Monnier, J., Ryan, U.S. and Nick, H.S. (1992) *Biochem. Biophys. Res. Commun.* **188,** 453.

Wagner, U.G., Pattridge, K.A., Ludwig, M.L., Stallings, W.C., Werber, M.M., Oefner, C.,Frolow, F., and Sussman, J.L. (1993) *Protein Sci.* **2**, 814.

Whittaker, J.W. and Whittaker, M.M. (1991) *J. Am. Chem. Soc.* **113**, 5528.

Whittaker, M.M. and Whittaker, J.W. (1997) *Biochemistry* **36**, 8923.

Wilson, G.S. (1978) *Methods Enzymol.* **54**, 396.

Wong, G.H.W., McHugh, T., Weber, R., and Goedell, D.V. (1991) *Proc. Natl. Acad. Sci. USA* **88**, 4372.

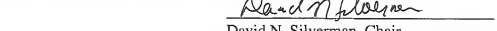
Yahara, O., Hashimoto, K., Taniguchi, N., Ishikawa, M., Sato, Y., Yamashita, H. and Ohno, H. (1991) *Res. Commun. Chem. Pathol. Pharmacol.* **72,** 315.

Yoritaka, A., Hattori, N., Mori, H., Kato, K., and Mizuno, Y. (1997) *J. Neurol. Sci.* **148,** 181.

BIOGRAPHICAL SKETCH

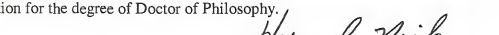
Vincent Lévêque was born on October 7, 1972, in Grenoble, France, where he remained through high school. In the fall of 1991, he began undergraduate training at the Euro-American Institute of Technology in Sophia-Antipolis, France. He transferred in 1993 to the Florida Institute of Technology in Melbourne, Florida, where he received his Bachelor of Science in biochemistry with high honors in May 1995. In the fall of 1995, he entered the graduate program in the Department of Biochemistry and Molecular Biology at the University of Florida. There, he worked with Dr. Silverman and Dr. Nick on studies of the kinetics and redox properties of human manganese superoxide dismutase. After receiving the Ph.D. from the University of Florida, he will continue as a postdoctoral fellow in the laboratory of Dr. Silverman for a few months, while applying for postdoctoral positions that focus on gene regulation and/or gene therapy. His long term goal is to use the numerous techniques and experiences acquired during his graduate school and postdoctoral experiences to direct a research laboratory in an academic institution.

I certify that I have read this study and that in my opinion it conforms to acceptable standards of scholarly presentation and is fully adequate, in scope and quality, as a dissertation for the degree of Doctor of Philosophy.



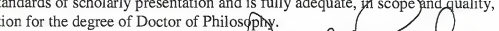
David N. Silverman, Chair
Distinguished Professor of Pharmacology and Therapeutics

I certify that I have read this study and that in my opinion it conforms to acceptable standards of scholarly presentation and is fully adequate, in scope and quality, as a dissertation for the degree of Doctor of Philosophy.



Harry S. Nick, Cochair
Professor of Neuroscience

I certify that I have read this study and that in my opinion it conforms to acceptable standards of scholarly presentation and is fully adequate, in scope and quality, as a dissertation for the degree of Doctor of Philosophy.



Daniel L. Purich
Professor of Biochemistry and Molecular Biology

I certify that I have read this study and that in my opinion it conforms to acceptable standards of scholarly presentation and is fully adequate, in scope and quality, as a dissertation for the degree of Doctor of Philosophy.



Arthur S. Edison
Assistant Professor of Biochemistry and Molecular Biology

I certify that I have read this study and that in my opinion it conforms to acceptable standards of scholarly presentation and is fully adequate, in scope and quality, as a dissertation for the degree of Doctor of Philosophy.



Benjamin A. Horenstein
Associate Professor of Chemistry

This dissertation was submitted to the Graduate Faculty of the College of Medicine and to the Graduate School and was accepted as partial fulfillment of the requirements for the degree of Doctor of Philosophy.

August, 2000

Dean, College of Medicine

Dean, Graduate School